hydrology

MDPI

Article

Hydrological Sustainability of Dam-Based Water Resources in a Mediterranean Basin Undergoing Climate Change

Nicola Montaldo *, Serena Sirigu, Riccardo Zucca, Adriano Ruiu and Roberto Corona

Dipartimento di Ingegneria Civile, Ambientale e Architettura, Università di Cagliari, 09123 Cagliari, Italy; serena.sirigu@unica.it (S.S.); rzucca@unica.it (R.Z.); adriano.ruiu@gmail.com (A.R.); roberto.corona@unica.it (R.C.)

* Correspondence: nmontaldo@unica.it; Tel.: +39-070-675530

Abstract: The Flumendosa dams are a key part of the water resources system of the island of Sardinia. The analysis of a long-term (1922–2022) hydrological database showed that the Flumendosa basin has been affected by climate change since the middle of the last century, associated with a decrease in winter precipitation and annual runoff (Mann–Kendall $\tau = -0.271$), reduced by half in the last century, and an increase in the mean annual air temperature (Mann–Kendall $\tau = +0.373$). We used a spatially distributed ecohydrological model and a water resources management model (WARGI) to define the economic efficiency and the optimal water allocation in the water system configurations throughout the evaluation of multiple planning and management rules for future climate scenarios. Using future climate scenarios, testing land cover strategies (i.e., forestation/deforestation), and optimizing the use of water resources, we predicted drier future scenarios (up to the end of the century) with an alarming decrease in water resources for agricultural activities, which could halt the economic development of Sardinia. In the future hydrological conditions (2024–2100), irrigation demands will not be totally satisfied, with up to 74% of future years being in deficit for irrigation, with a mean deficit of up to 52% for irrigation.

Keywords: water resources management; climate change; ecohydrological model; long-term hydrological database; dams

Citation: Montaldo, N.; Sirigu, S.; Zucca, R.; Ruiu, A.; Corona, R. Hydrological Sustainability of Dam-Based Water Resources in a Mediterranean Basin Undergoing Climate Change. *Hydrology* **2024**, *11*, 200. https://doi.org/10.3390/hydrology11120200

Academic Editor: Yanfang Sang

Received: 30 October 2024
Revised: 16 November 2024
Accepted: 19 November 2024
Published: 25 November 2024

1. Introduction

Over the past century, climate change has been altering precipitation and air temperature regimes across the world [1–5]. The Mediterranean region is considered to be one of the most pronounced "hot spots" in the world, highly sensitive to climate change [6]. While air temperature is increasing, precipitation and runoff are mainly decreasing in Mediterranean regions, impacting water resource conditions [7–10]. In Sardinia, one of the largest islands in the Mediterranean Sea, ref. [9] estimated a persistent negative trend of winter precipitation (Mann–Kendall τ up to -0.40) in the 1922–2010 period, which produced an even more dramatic negative trend of runoff (Mann–Kendall τ up to -0.45), with runoff more than halved in recent decades and a decrease in the mean annual basin runoff coefficient (Mann–Kendall τ value of -0.32; Montaldo and Oren [11]). Runoff is a key term in basin water resources and a good indicator of water availability [12,13]. Indeed, the impact on water resources has been dramatic in Sardinia in recent decades, with frequent water supply restrictions, including domestic consumption [14]. A further negative precipitation trend and warmer conditions have been predicted for the near future [15–18], affecting the central Mediterranean basin and further intensifying the desertification process [11,15,19–24].

Nowadays, long-term databases of land-observed hydrologic data (e.g., rain, runoff, and air temperature) have been available for most of the last century [25–27], and so the impact of past climate change on water resources can be evaluated [28,29]. Ecohydrological models are a key tool for predicting climate impacts on the state of water resources and

land cover dynamics through the coupling of hydrologic and vegetation dynamics models at the basin scale with a spatially distributed approach [24,30–36]. The availability of a long-term hydrological database is important for the accurate calibration and validation of ecohydrological models, which, when well validated, are a robust tool for predicting the impacts of future climate change scenarios. The availability of future climate scenarios [15,37] predicted by global circulation models (GCM), e.g., in the reports of the Intergovernmental Panel on Climate Change (IPCC) [37], when coupled with robust ecohydrological models, allows the prediction of the state of water resources and their interactions with vegetation and land surface fluxes up to the end of the century [38–40].

In Mediterranean regions under scarce water conditions, water resource management models have, historically, been developed for optimizing water uses and demands [41–43]. Irrigated agriculture accounts for around 85–90% of global water consumption, making it the largest consumer of water globally [44]. Climate change will have a profound impact on irrigation water supply and demand, especially in the Mediterranean basin, as shown by Eekhout et al. [45] in southeastern Spain and by Lyra and Loukas [46] in Greece. Examples of water resource management are in those areas with scarce water resources but with favorable conditions for population growth, irrigation, and tourism, like countries in the Mediterranean Sea basin, California, and Australia, which developed a long tradition of adaptation to irregular water resources [42]. Water resource management models are a required tool for optimizing water uses (e.g., irrigation, drinking, and industrial activities) under definite hydrological conditions [41,47–50]. In Mediterranean regions, the rainfall regime has strong seasonality, with wet months in autumn and winter producing most of the runoff and aquifer recharge, in contrast to dry spring and summer months [9,51,52]. This seasonality has historically determined the needs of the hydraulic infrastructure required to make water resources available, being produced in the wet months for the whole year [42]. Storage infrastructure in regions under water scarcity conditions has been built in the last century, producing an increase in water availability, and water resources management models allowed the optimization of water demands [42]. The sustainability of current water resource management systems is under pressure due to recent climate change impacts and the growth of water use needs. Water resource planning needs to be updated and adapted to the predicted future water resource scenarios and uses. Future water resource scenarios can be predicted by the coupling of future GCM climate scenarios and ecohydrological models; water resource management models can allow the evaluation and optimization of water uses under predicted hydrological scenarios.

Considering future water resource scenarios, water resources planning needs to consider both the impact of environmental strategies (e.g., land cover change) in the contributing basin and potential changes in water demands according to social and economic growth politics [53]. Land cover change strategies, such as afforestation or deforestation, can impact the environment and water resource conditions of the basin. Forests are important for carbon sequestration, erosion control [54], and runoff production [55]. A reduction in forest cover may lower soil water infiltration [55], increasing surface runoff with implications on the water yield at a catchment scale [56–58]. From a water resource perspective, a forest cover reduction may be positive, in contrast with the afforestation strategies for contrasting global warming [56,58]. Recently, Hou et al. [59] compared the hydrological sensitivity to deforestation and afforestation of multiple watersheds across the globe and concluded that the water-limited watersheds have the largest hydrological sensitivities. Land cover strategies under climate change are, therefore, still questioned and need to be analyzed further. At the same time, future water uses can change in relation to regional social and economic growth policies [53]. Agricultural and industrial water demands may still be growing in the economic plans of Mediterranean regions [42], but these challenging increases in water use need to be consistent with available water resources and water demands for ecological river conservation.

Studying the impacts of climate change on Sardinia is interesting because of its position in the center of the Mediterranean Sea, its high sensitivity to climate change [9,11,23,60],

its relatively low urbanization and human activity (with ~50% of the total area covered by forest [61]), and the lack of relevant land cover changes [24]. In the dry seasons, water use is typically higher due to agricultural needs (for irrigation), domestic use, and tourism-related uses. To satisfy the Sardinian water resources needs, an artificial reservoir system spread over the whole island was designed one century ago [62] and improved over time [63]. This artificial reservoir system was a key point in the economic development and growth of Sardinia in the nineteenth century, enabling it to support the increase in industry, tourism, and agriculture [64,65]. In particular, agricultural uses are still predominant (60–70% of total water consumption in Sardinia), although the growth of domestic and tourist demands occurred as the population increased after the second-world war and with the expansion of tourism in recent decades [14,65]. Recent droughts [9] and drier future climate conditions may undermine the Sardinian water resource management system, not allowing it to satisfy the water demand and slowing its economic growth.

The Flumendosa water resource system is a well-suited Sardinian case study because of its long-term hydrological database (1922–2022) and the major reservoir system (about 620×10^6 m^3 total capacity). The reservoir system supplies the main Sardinian plain and irrigated area, the Campidano, and the main city (Cagliari); it has been crucial for the economic development of Sardinia since the last century [10,62,64]. Our objectives are as follows: (1) to evaluate past climate impacts on basin water resources using the Flumendosa basin's long historical hydrological database; (2) to predict future water resources and use conditions through a proposed approach that couples a distributed ecohydrological model, a water resources management optimization (WARGI) model, and the IPCC's future climate scenarios; and (3) to provide directions on the impact of simplified land cover change strategies on future scenarios of water resources management.

2. Materials and Methods

2.1. The Ecohydrological Model and the Water Resource Management System

We used an ecohydrological distributed model and a water resource management model (WARGI) (Figure 1), which are described below; their coupled use in the proposed approach is also outlined. The ecohydrological model predicts the basin soil water balance and the runoff, which fills the reservoir system and is the input of WARGI, which optimizes reservoirs and water uses. WARGI manages a multi-reservoir system and the water demands, which can be irrigation, civil, industrial, and environmental.

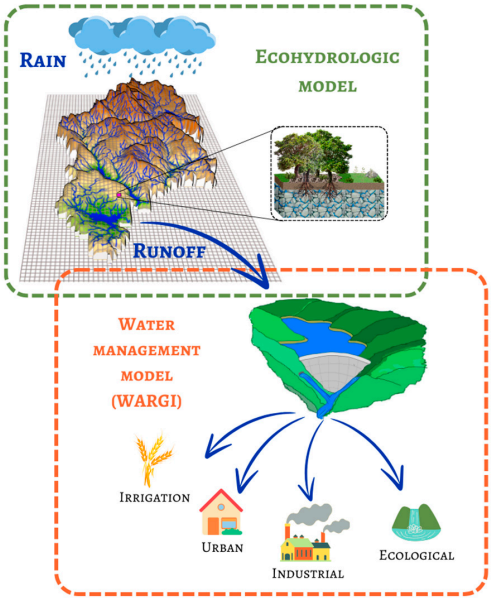

Figure 1. The schemes of the distributed ecohydrological model and the water resources management model (WARGI).

The use of the coupled models allowed us to predict the future scenarios of water resource management and the optimal water allocation in the system configurations for water demand and land cover change scenarios.

2.1.1. The Distributed Ecohydrological Model

The spatially distributed ecohydrological model (Figure 2) couples a hydrological model and a vegetation dynamics model, as derived from the [24] model. The model runs at a daily timescale and 200 m spatial resolution. Three principal components can be identified in the model (Figure 2): (1) the soil water balance model (SWBM) that computes soil moisture, water balance, surface runoff, and subsurface water flux; (2) the vegetation dynamic model (VDM) that computes biomass budgets and leaf area index (LAI); and (3) the simplified overland flow and base flow computations.

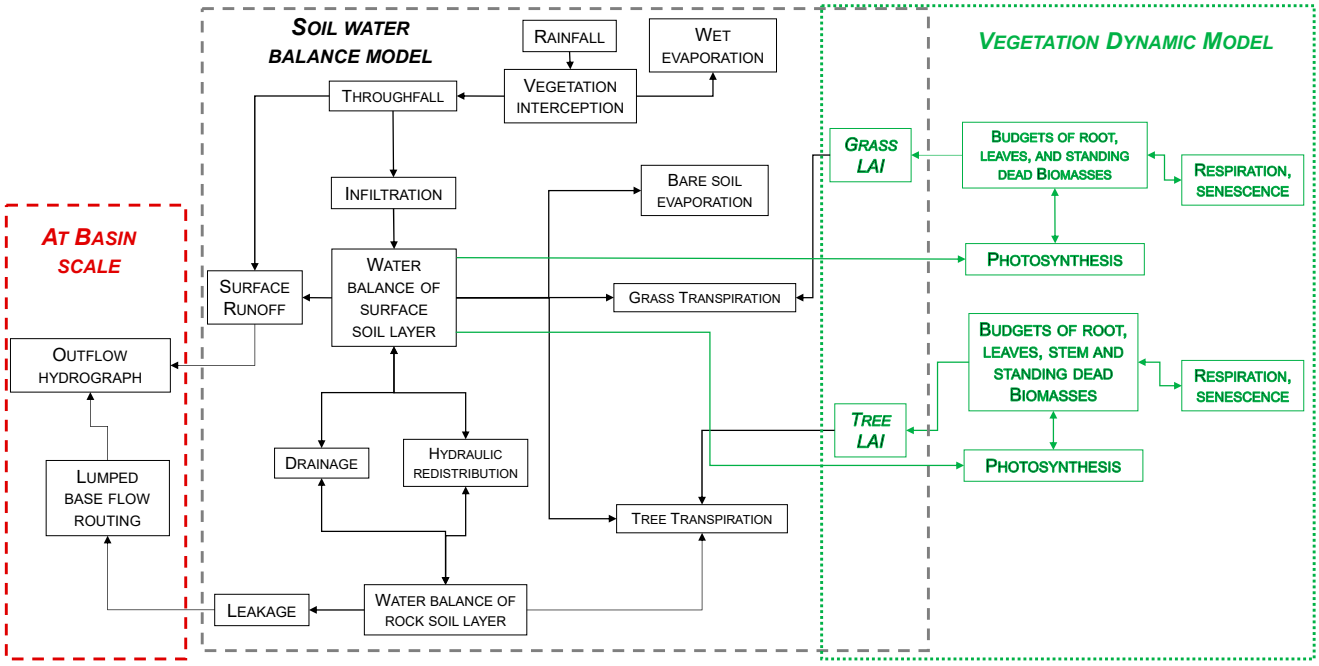

Figure 2. The flowchart of the distributed ecohydrological model.

In the first component, the soil water budget is computed for each cell of the basin. From this model component, the surface runoff and drainage are predicted and used by the third component of the model to compute runoff at the basin scale. The second component, the vegetation dynamics model, provides the *LAI* at each cell, which is used by the SWBM for computing the evapotranspiration (*ET*) and rain interception (Figure 2). The meteorological model inputs are precipitation (*P*), air temperature (T_{air}), wind speed (*WS*), relative humidity (*RH*), incoming short-wave solar radiation (R_{sw}), and photosynthetically active radiation (*PAR*). We used the Thiessen method for the spatial interpolation of the meteorological model inputs. The parameters of the model are provided in Table 1.

Table 1. Ecohydrological model parameters for the Flumendosa basin.

Parameter	Description	Grass	Forest
$r_{s,min}$ [s m^{-1}]	Minimum stomatal resistance	150	290
θ_{wp} [-]	Wilting point	0.08	0.05
θ_{lim} [-]	Limiting soil moisture for vegetation	0.20	0.18
T_{min} [°K]	Minimum temperature	279.15	268.15

Table 1. *Cont.*

Parameter	Description	Grass	Forest
T_{opt} [°K]	Optimal temperature	293.15	288.15
T_{max} [°K]	Maximum temperature	299.15	304.15
c_a [m^2 gDM^{-1}]	Specific leaf areas of the green biomass	0.01	0.0065
c_d [m^2 gDM^{-1}]	Specific leaf areas of the dead biomass	0.01	0.0062
k_e [-]	PAR extinction coefficient	0.5	0.5
ξ_a [-]	Parameter controlling allocation to leaves	0.6	0.55
ξ_s [-]	Parameter controlling allocation to stem	0.1	0.1
ξ_r [-]	Parameter controlling allocation to roots	0.4	0.35
Ω [-]	Allocation parameter	0.8	0.1
m_a [d^{-1}]	Maintenance respiration coefficients for aboveground biomass	0.032	0.0001
g_a [-]	Growth respiration coefficients for aboveground biomass	0.32	0.85
m_r [d^{-1}]	Maintenance respiration coefficients for root biomass	0.007	0.0003
g_r [-]	Growth respiration coefficients for root biomass	0.1	0.1
Q_{10} [-]	Temperature coefficient in the respiration process	2.5	3
δ_a [d^{-1}]	Death rate of aboveground biomass	0.023	0.0019
δ_r [d^{-1}]	Death rate of root biomass	0.005	0.0001
k_a [d^{-1}]	Rate of standing biomass pushed down	0.23	0.35
Q_N [-]	Soil respiration coefficient related to temperature	1.2	
R_{10} [mmol CO_2/m^2 s]	Reference respiration at 10° C	2.54	
$z_{om,v}$ [m]	Vegetation momentum roughness length	0.05	0.5
$z_{ov,v}$ [m]	Vegetation water vapor roughness length	z_{om}/7.4	z_{om}/2.5
$z_{om,bs}$ [m]	Bare soil momentum roughness length	0.015	
$z_{ov,bs}$ [m]	Bare soil water vapor roughness length	z_{om}/10	

The Soil Water Balance Model

The SWBM predicts land surface fluxes and soil moisture evolutions for each grid cell. It is derived from the models in [24,66,67] and includes three land surface components for each cell: bare soil, grass, and trees. The model includes two vertical layers: a surficial soil of variable depth (d_s) according to the soil depth of the cell and an underlying layer with d_r depth. In the following, the soil water balance is described because it is updated here to include a soil sublayer or a root-accessible fractured rock sublayer according to the soil depth below the surficial soil layer. The soil water balance model for the root zone can include a soil sublayer or a root-accessible fractured rock sublayer according to the soil depth (if it is greater or lower than 1 m, respectively [68]). The model simulates the water balance of the two layers for each cell:

$$d_s \frac{\partial \theta_s}{\partial t} = P - E_w - Q_{sup} - f_{bs}E_{bs} - f_g E_g - \xi_t \, f_t E_{t,s} + f_d - D_r \quad (1)$$

$$d_r \frac{\partial \theta_r}{\partial t} = D_r - f_d - (1 - \xi_t) f_t E_{t,r} - L_e \quad (2)$$

where θ_s is the moisture of the upper soil layer, θ_r is the moisture of the underlying soil/rocky layer, P is the precipitation, Q_{sup} is the surface runoff, E_w is the wet evaporation (which is equal to the rainfall interception, characterized by a storage capacity of 0.2 LAI [69]), E_{bs} is the bare soil evaporation, E_g is the grass transpiration, $E_{t,s}$ is the tree transpiration from the surface soil layer, $E_{t,r}$ is the tree transpiration from the underlying layer (with tree transpiration, $E_t = E_{t,s} + (1 - \xi_t) E_{t,r}$), ξ_t is the percentage of tree root water uptake from the surface soil layer, f_d is the daily hydraulic redistribution flux between the surface soil and the underlying layer through the tree roots, D_r is the vertical drainage, L_e is the leakage, and f_{bs}, f_g, and ft are the fractions of bare soil, grass cover, and tree cover in each cell, respectively, with $f_{bs} + f_g + f_t = 1$. Q_{sup} is estimated using the Soil Conservation Service Curve Number (SCS-CN) method [70–73] from P, and the antecedent moisture conditions from the rain in the previous five days are computed [24]. D_r and L_e are estimated

using the unit gradient assumption of gravity drainage [74] and related to soil moisture, as follows [75]:

$$D_r = k_{sat,s}\left(\frac{\theta_s}{\theta_{sat,s}}\right)^{2b_s+3} \quad (3)$$

$$L_e = k_{sat,r}\left(\frac{\theta_r}{\theta_{sat,r}}\right)^{2b_r+3} \quad (4)$$

where $k_{sat,s}$ and $k_{sat,r}$ are the saturated hydraulic conductivity of the surficial soil layer and the deeper layer, respectively, b_s and b_r are the slopes of the soil retention curve of the two layers, and $\theta_{sat,s}$ and $\theta_{sat,r}$ are the saturated soil moisture of the two layers. The f_d contribution is estimated as a function of the soil moisture gradient between the surface and underlying sublayer through the following [67,76]:

$$f_d = a_f(\theta_r - \theta_s)^{b_f}, \quad (5)$$

where a_f and b_f are tree root parameters. Evapotranspiration components (E_g, $E_{t,s}$, and $E_{t,r}$) are estimated by the Penman–Monteith equation ([77], Equation (10.34)), with the canopy resistance (r_c) given by Jarvis et al. [78]:

$$r_c = \frac{r_{s,min}}{LAI}[f_1(\theta)f_2(T_a)f_3(VPD)]^{-1} \quad (6)$$

where f_1, f_2, and f_3 are stress functions of soil/rock moisture, air temperature, and VPD [11,24,33]. Bare soil evaporation is estimated as a function of soil moisture through $E_{bs} = \alpha\ PE$ [79], and PE is the potential evaporation based on Penman–Monteith [80] (Equation (10.15)). Total evapotranspiration is given by the following:

$$ET = f_{bs}E_{bs} + f_g E_g + \xi_t\ f_t E_{t,s} + (1-\xi_t)f_t E_{t,r} + E_w \quad (7)$$

The Vegetation Dynamics Model

The VDM computes the change in biomass over time, from the difference between the rates of biomass production (photosynthesis) and loss, such as occurs through respiration and senescence [81,82]. The VDM distinguishes between trees and grass components and was derived by [31,33] from the Nouvellon et al. [83] model.

In the VDM of trees, four separate biomass states (compartments) are tracked (green leaves, stems, living roots, and standing dead), while the VDM of the grass cover distinguishes only three of these biomass compartments (green leaves, roots, and senesced aboveground components; Table S1). The model equations are provided in Table S1, and the parameters are provided in Table 1. The leaf area index is estimated from the biomass through linear relationships ([30,31,33,83]; Table S1).

The key term of the VDM, photosynthesis P_g, is computed using the approach in [31], which includes the canopy resistance estimated through (6), linking P_g to soil moisture. Hence, P_g accounts for the contributions of two water sources: the surface root zone and the underlying sublayer down to the reach of tree roots. Details on the estimates of the VDM terms are provided in [33]. Carbon exchange rates for each vegetation component are computed as the difference between P_g and respiration (see Table S1; [66]). The VDM provides estimates of daily values of leaf biomass and, thus, the *LAI* of the trees and grass. In turn, this is then used by the SWBM to estimate evapotranspiration, energy flux, rainfall interception, and the soil water content in the root zone at half-hour intervals (Figure 2). The SWBM provides soil moisture and aerodynamic resistance to the VDM (Figure 2).

The Surface Runoff and Base Flow

In each cell of the basin, the Q_{sup} surface runoff is computed daily by the SWBM, and the total surface runoff at the basin scale is computed by summing the daily surface runoff contribution of the cells in the basin. Following [84], the Q_b subsurface flow at the basin

outlet is computed at the $j + 1$ time step through a lumped conceptual approach, namely a linear reservoir method [85]:

$$Q_b^{j+1} = Q_b^j \, e^{-\Delta t/\kappa} + L_e^{j+1}\left(1 - e^{-\Delta t/\kappa}\right) \quad (8)$$

where Δt is the time step (=daily) and k is a linear reservoir parameter. At each daily time step, the total runoff at the basin outlet (Q) is given by the sum of total surface runoff and Q_b.

2.1.2. Water Resources Management

WARGI is a Decision Support System that was developed by [63,86,87] to provide a tool to analyze the behavior and performance of a complex water resource system. It was developed to manage the requirements of multi-reservoir systems under water scarcity conditions, as frequently occur in Mediterranean regions [41]. Water allocation in the WARGI is retrieved via user-defined preferences for supply sources and priorities for demand centers; the water flows in the system are evaluated by considering an optimal path search procedure. Additionally, the user can define reserved storage in reservoirs, the withdrawal of water from which is managed to satisfy user-selected higher-priority demands.

The water resource system can be viewed as a physical network where the nodes and arcs are as follows:

- Reservoir nodes: These represent surface water resources with storage capacity. In these nodes, losses by evaporation can be considered;
- Demand nodes: For irrigation, civil, and industrial, among others;
- Hydroelectric nodes: They are non-consumptive nodes associated with hydroelectric units;
- Confluence nodes: Such as river confluence, withdraw connections for demands satisfaction, etc.;
- Aquifer nodes: These nodes represent ground water resources with storage capacity;
- Natural stream arcs: These represent the natural runoff along rivers or river beds;
- Conveyance work arcs: These are artificial channels, such as ditches, pipes, etc.;
- Water pumping facility arcs: These are arcs with a pumping plant;
- Emergency transfer arcs: These arcs allow transfers of water to alleviate shortages;
- Recharge facility arcs: These allow the direct injection of surface water from a connection node into an aquifer;

Some of the operational management issues to consider in the problem can be easily modeled using graph structures as follows:

- Priorities in the stored water level of reservoirs;
- Priorities in demand satisfaction of demand nodes;
- Penalty on shortage and emergency transfers;
- Water quality aspects related to storage conditions.

The planning issues refer to the design of the physical system with dimensions associated with future works: reservoir capacities, pipe dimensions, irrigation areas, etc.

2.1.3. The Coupling of the Ecohydrological and Water Resource Management Models

To predict future scenarios of water resources and use conditions, we coupled the distributed ecohydrological model with the WARGI model (Figure 1). In general, by using meteorological inputs, the ecohydrological model predicts the runoff that fills the reservoir system, and that is the input of the water resource management model, which optimizes reservoirs and water uses. When the meteorological inputs are derived from the IPCC future climate scenarios, the coupled models predict the future scenarios of water resource management.

2.2. The Flumendosa Basin Case Study

2.2.1. Basin Characteristics

The Flumendosa basin, located in central–eastern Sardinia (9.33° E, 39.8° N), is the second longest river of the region with a length of 127 km (Figure 3), a mean elevation of 721 m a.s.l., a mean slope of 11%, and an area of 1017 km^2 at the Monte Scrocca section. The northern part of the basin is mountainous, with steep hillslopes and higher rainfall compared to the southern part. The reservoir system includes two large dams, the Flumendosa dam at Nuraghe Arrubiu (reservoir capacity of 300 × 10^6 m^3) and the Mulargia dam at Monte Su Rei (reservoir capacity of 320 × 10^6 m^3) (Figure 3). The two reservoirs are interconnected by an underground conduit to increase the collection of the runoff coming from the Nuraghe Arrubiu dam basin (751 km^2), which is much larger than the Mulargia basin (180 km^2). The total capacity of the reservoir system is 620 × 10^6 m^3, one of the largest reservoir capacities in Europe. Due to its key role in the Sardinian water resource system, the Flumendosa basin became an experimental basin of the University of Cagliari [10,33,66,88], resulting in an extensive hydrological database.

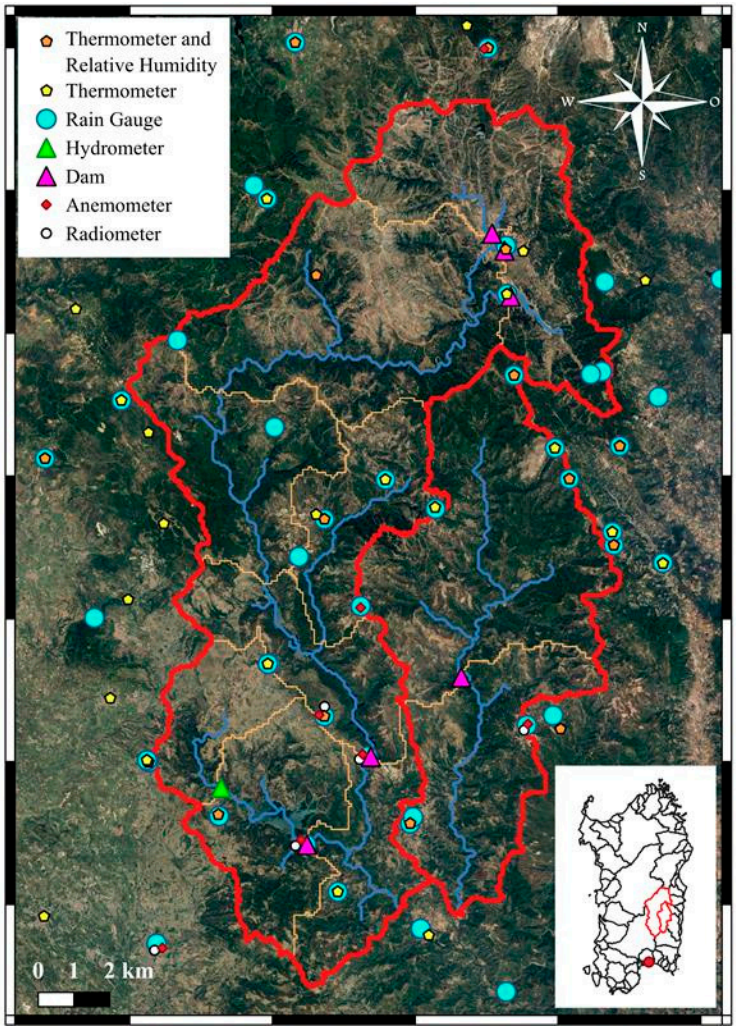

Figure 3. The Flumendosa basin with the positions of the rain gauges, the meteorological stations, the hydrometers, and the dams.

The climate regime is typically Mediterranean, the mean annual precipitation is 885 mm, and the mean annual air temperature is 14.21 °C. The soil thickness in the basin generally ranges from 5 to 200 cm with an average depth of 44 cm with deeper soils in the valley and thin soil in the steep slopes; the soil texture is mainly silt loam soils in

the valley with the mountainous part dominated by exposed rocks. The land use is also inhomogeneous, with forested and natural areas predominant in the north and agricultural activities and grazing areas in the south (downstream) due to thicker soils. The urbanization is negligible (≈2.31%) in the basin, while forested areas are predominant (=57%). The spatial distribution of the tree cover in the basin (spatial resolution of 200 m) was estimated from Sentinel 2 remote sensing data using the Scene Classification Mask (SCL) product (Figure S1).

2.2.2. Hydrologic Data

Daily precipitation data from 41 rain gauge stations in and surrounding the Flumendosa basin and monthly runoff data at the basin outlet were collected for the period 1923–2022 (Figure 3). Data were collected from the Sardinian environmental protection agency and the Sardinian water resources authority. Data were processed, and the linear regression method was used for gap-filling (using the data collected at the gap time in the nearby consistent station). Runoff data are also available for the Mulargia section for a shorter period (2003–2007). Air temperature data from 13 stations are available at the daily scale (Figure 3) from 1924, and air temperature and relative humidity data from 16 stations are available from 2011, at 30 min intervals. Incoming short-wave radiation data are available from 2007 (from 5 stations at 30 min intervals), and wind speed data are available from 1973, at an hourly timescale at 4 stations.

Data from two eddy-covariance-based micrometeorological stations at Orroli and Nurri are also available [66]. The Orroli site is located in east–central Sardinia (39°41′12.57″ N, 9°16′30.34″, 500 m elevation), with thin soils (mean soil depth of 15 cm) and has been monitored since 2003. The vegetation is a patchy mixture of wild olive tree (Olea Sylvestris) clumps with canopy cover of ~33% and herbaceous seasonal species. Data for sensible heat flux, evapotranspiration, and CO_2 exchanges are available [89]. The second site is at Nurri (39°41′11.51″ N, 9°12′57″ E). The soil is mainly silty clay loam (17.7% sand, 52.2% silt, 30.3% clay), and the soil depth is more than 1.5 m. The site is located in an alluvial plain valley of the Mulargia river, a subbasin of the Flumendosa. It is a C3 grass site with a maximum height of 70 cm during the spring season. Data are available for the 17 April 2003–30 September 2005 period only. For a historical hydrological analysis from 1923, data of relative humidity, wind velocity, and incoming solar radiation were collected from the ERA5 European Centre for Medium-Range Weather Forecasts (ECMWF) atmospheric reanalysis datasets [90,91], which have been successfully validated using 13 years of data of wind velocity from the Orroli station (RMSE = 1 m/s), 13 years of incoming solar radiation data from the Orroli station (RMSE = 35 W/m^2), and 5 years of data of relative humidity from the Orroli station (RMSE = 10%).

2.3. The WARGI Model of the Flumendosa Case Study

WARGI was applied to the Flumendosa water resources system, including 14 nodes, 13 arcs, 3 reservoirs, 4 demands (urban, industrial, irrigation, and environmental), and 2 confluences. WARGI is the actual water resource management system of the Sardinian water resources authority [41]. In the Flumendosa water resources system, the total annual demand is an average of ≈240 million cubic meters, with predominantly irrigation (48%) and civil uses (31%). In Table 2, the WARGI rules of priority for water use, in the case of water restrictions in the Flumendosa reservoir system, are reported; first priority is given to civil demands, then industrial demands, which are, however, lower than civil and irrigation demands. These rules are the official rules for the Flumendosa water resources system, managed by the Sardinian water authority (ENAS), and have been preserved in our study.

Table 2. The rules of priority classification of water uses in the Flumendosa reservoir system.

Class	Civil	Industrial	Irrigation	Ecological
I	50			
II	30	80		
III	20	20	50	50
IV			50	
V				50

2.4. Future Climate Scenarios

For future climate scenarios, we considered the IPCC scenarios of the Sixth Assessment report [92]. We tested the historical time series of precipitation and air temperature from 17 Global Climate Models (GCMs), comparing the mean annual variation of the two variables for the period 1983–2014 compared to the period 1950–1982. We selected the MPI-ESM1-2-LR, which better represented the historical period (historical variation of the Flumendosa mean annual precipitation: ΔPy Flumendosa = −14.16%, ΔP_y MPI-ESM1-2-LR = −8.70%, historical variation of the Flumendosa mean annual air temperature: ΔT_y Flumendosa = +0.40 °C, ΔT_y MPI-ESM1-2-LR = +0.36 °C), compared to other 16 GCMs (Figure S2), and provided complete datasets of precipitation, temperature, relative humidity, wind velocity, and incoming solar radiation. We considered two future scenarios of high emissions (MPI-ESM1-2-LR SSP3-RCP7.0, MPI-ESM1-2-LR SSP5-RCP8.5).

Future climate scenarios were generated for the Flumendosa basin up to the year 2100 from the GCM predictions through the multivariate bias correction technique [93], which uses the land-observed meteorological data of the past to estimate the required statistics. The reference period is from 1925 to 2014. The multivariate bias correction technique uses an iterative algorithm that consists of three main steps: (1) constructing a uniformly distributed random orthogonal rotation matrix and applying it to the land-observed meteorological target data and to the GCM meteorological source data from the past; (2) correcting the marginal distributions of the rotated source data by using an empirical quintile map; and (3) applying the inverse rotation to the resulting data. These steps are repeated until the multivariate distribution converges to the target distribution. The multivariate bias correction allowed us to statistically downscale GCM data at the resolution of 1.25° latitude and 1.87° longitude (~150 km) to the Flumendosa basin.

2.5. Land Cover Change and Water Usage Strategies

For investigating the impact of land cover change strategies (e.g., increase/decrease in tree cover distribution) on soil water and runoff in future climate scenarios, we developed two opposite land cover strategies: an afforestation process and a deforestation process. The afforestation was predicted in those land areas of the basin where, due to human activities, the forested areas were removed in the past, particularly in the plain areas (Figure S1). The afforestation and deforestation land cover strategies increase and decrease the fraction of tree cover of the basin by 33% and 22%, respectively, compared to the actual state (mean value of 0.57; Figure S1).

Considering the potential socio-economic growth scenarios of Sardinia, mainly related to the growth of agricultural water usage, we identified three future water use scenarios based on historical water demands (Table 3): scenario A (242.1 × 10^6 m^3), which confirmed the mean water demands of the 2019–2021 period; scenario B (279.6 × 10^6 m^3), which assumed a demand equal to the maximum annual water demands of the 2012–2021 period; and scenario C (364.0 × 10^6 m^3), with further higher water demands. Irrigation demands are predominant and increased in all three scenarios (48% for scenario A, 49% for scenario B, and 61% for scenario C; Table 3).

Table 3. The yearly water demands of civil, industrial, irrigation, and ecological uses for water demand scenarios A, B, and C.

Demand Scenario	Total Demand	Civil Demand				Industrial Demand	Irrigation Demand			Ecological Demand
		South Sardinia	Orroli	Gerrei	TOTAL Demand		South Sardinia	Isili	TOTAL Demand	
	[mm³/y]	[mm³/y]	[mm³/y]	[mm³/y]	[mm³/y]	[mm³/y]	[mm³/y]	[mm³/y]	[mm³/y]	[mm³/y]
A	242.1	73.1	0.5	0.9	74.5	12.2	115.0	1.2	116.2	10% of the runoff
B	279.6	86.6	0.8	1.0	88.4	14.5	136.2	1.3	137.5	
C	364.0	86.6	0.8	1.0	88.4	14.5	220.6	1.3	221.9	

2.6. Comparisons and Statistical Data Analysis

Data were analyzed using monthly, seasonal, and yearly time scales. For annual computations, we used the hydrologic year beginning in Sardinia in September, the end of a typical dry summer. The runoff coefficient (Q/P, runoff/precipitation) was used for relating the runoff amount to the incoming precipitation amount, and an index of wetness (P/PE, precipitation/potential evaporation) was used for distinguishing annual meteorological conditions.

Model "goodness-of-fit" was evaluated by comparing modeling results with observations and using the following statistics: mean (μ), standard deviation (SD), coefficient of variation (CV), mean error (me), root mean square error (RMSE), correlation coefficient (ρ), and the Nash–Sutcliffe model efficiency coefficient (NSE).

Trends of the data are computed using the Mann–Kendall non-parametric test [94–96]. The Mann–Kendall τ measures the monotonic relationship between two x and y variables (in this study, the time, e.g., year, and the hydrological variable, e.g., precipitation), and it is less sensitive to outliers and missing data values. In the method, all data pairs are ordered by increasing x and analyzing how y varies; τ value will be positive if y values increase more often than they decrease, while τ will be negative if y values decrease more often than they increase. To evaluate τ, a parameter D has been evaluated as follows:

$$D = NP - M \tag{9}$$

where NP is the "number of pluses", the number of times y increases as x increases, and M is the "number of minuses", the number of times y decreases as x increases. Defining n as the number of elements of the time series and $n(n-1)/2$ as the number of possible comparisons, the Mann–Kendall τ coefficient is defined as follows:

$$\tau = \frac{D}{\frac{n(n-1)}{2}} \tag{10}$$

To verify the significance of the τ value, it is necessary for the null hypothesis to be rejected; for $n \leq 10$, an exact Mann–Kendall test is computed, while if $n > 10$, the test is modified to be approximated by a normal distribution [96]. Details are in Montaldo and Sarigu [9].

The Theil–Sen slope method is used to estimate the slope linear trends [97,98]. The estimator is also called the "median of pair-wise slope". Generally, this estimator is frequently applied in climatology and for the analysis of the hydrometeorological time series to define the rate of change. The β sign represents the direction of change, and its value indicates the steepness of change. The Theil–Sen method and the Mann–Kendall test are strongly connected; the β slope estimator is related to the Mann–Kendall τ test statistic, such that if $\tau < 0$, then $\beta \leq 0$, and if $\tau > 0$, then $\beta \geq 0$ because τ is equivalent to the number of positive D (Equation (1)) minus the number of negative D, and β is the median of these D. This estimator is widely used in hydrologic applications [99–102] because it is quite resistant to the effect of extreme values in the data.

3. Results

3.1. Analysis of Historical Hydrological Data

The annual rainfall in the Flumendosa basin significantly decreased in the last century (Mann–Kendall $\tau = -0.247$, $p < 0.005$, and Theil–Sen slope $\beta = -2.50$ mm/y), with mean annual precipitation reducing from 922 mm/y to 764 mm/y (Figure 4a). The decrease in rainfall is even higher if we consider that winter precipitation is the key to the water resources management system. Due to the precipitation regime in the basin (Figure 5a), precipitation is mainly concentrated in the autumn and winter months, with mean monthly precipitation ranging from 86 mm in March and 134 mm in December to 15 mm in July (Figure 5a); the decrease in precipitation was significant in winter (Mann–Kendall τ of -0.271 with $p < 0.005$, and Theil–Sen β of -0.52 mm/y; Figure 5b). On the other hand, the increase in air temperature was higher in the spring and summer months (Mann–Kendall τ up to 0.26 in summer; Figure 5c), when the air temperature was already much higher (up to 24 °C on average in summer; Figure 5a), in contrast with the colder winters (7.1 °C, on average in January). The negative trend of observed annual runoff was significant and higher than the negative trend of annual precipitation, reaching a Mann–Kendall τ of -0.276 ($p = 0.001$) and a Theil–Sen β of -2.337 mm/y (Figure 5b). In the 1990s and the first decades of the 2000s, annual runoff was very low, with values lower than 100 mm/y for three years (1995, 2002, and 2018) (Figure 4b). In contrast, the mean annual air temperature of the basin increased in the last century (Mann–Kendall $\tau = 0.37$, $p<0.005$ and Theil–Sen slope $\beta = +0.011$ °C/y), highlighting warmer conditions in the last decade, with an increase in air temperature of +0.55 °C (Figure 4c).

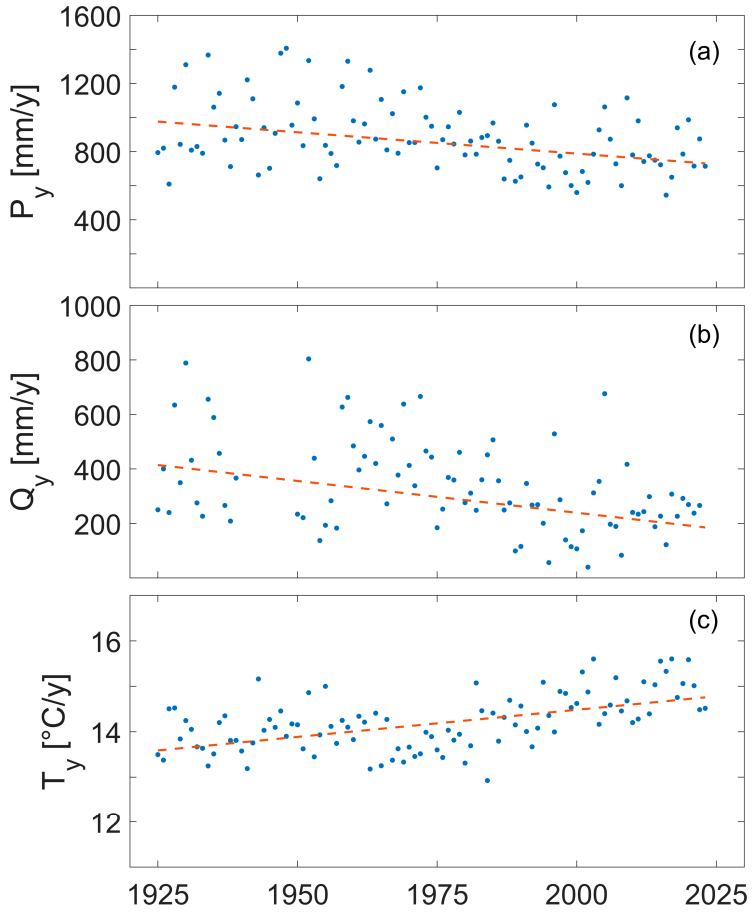

Figure 4. Annual series and trends of (**a**) precipitation (P_y), (**b**) runoff (Q_y), and (**c**) air temperature (T_y) at the Flumendosa basin. The slopes of the trend lines (red dashed) are estimated using the Theil–Sen method.

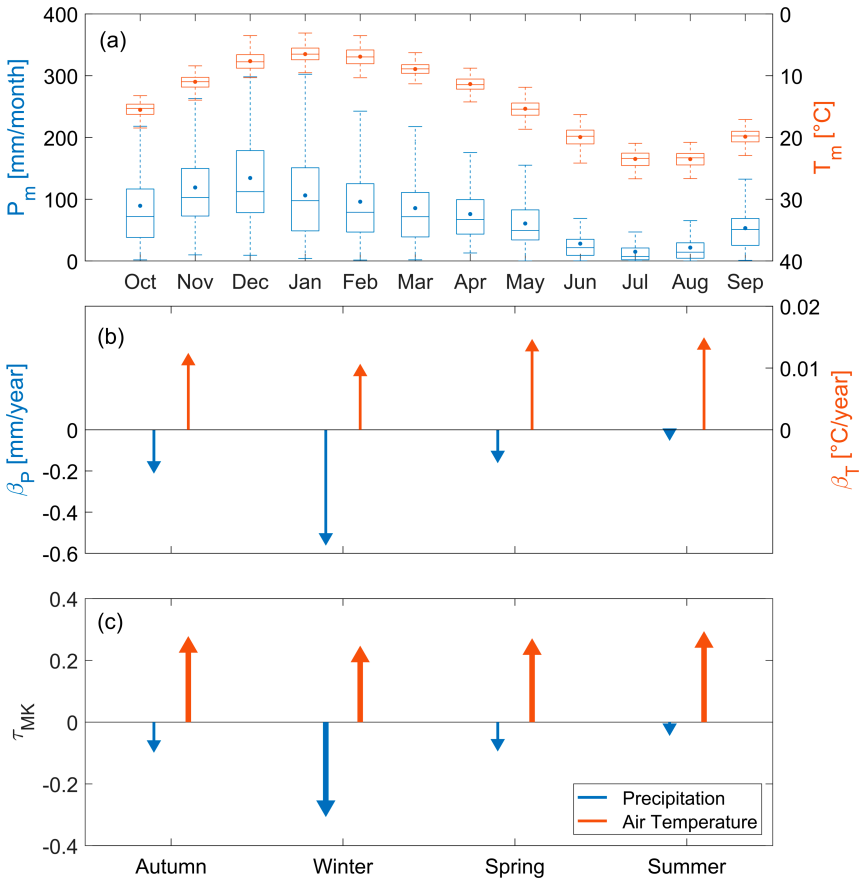

Figure 5. Historical climate at the Flumendosa basin: (**a**) monthly precipitation (P_m) and air temperature (T_m) regimes (the statistics of the 1924–2022 period are shown in each estimation box: filled circles indicate the means, the horizontal lines show the median, the box, and whiskers represent quartiles, and outliers are depicted individually); (**b**) the Theil–Sen β of the seasonal mean precipitation (β_P) and air temperature (β_T) trends; (**c**) the Mann–Kendall τ (τ_{MK}) of the seasonal mean precipitation and air temperature trends (thicker arrows when $p < 0.05$).

3.2. The Ecohydrological Model Results for the Historical Period

The distributed ecohydrological model was calibrated and validated at the Flumendosa basin (at Monte Scrocca), comparing the modeled and observed runoff for the longer 1925–2022 period (Figure 6a). Tables 1 and 4 report the values of the calibrated parameters: the CN of the SCS-CN method (the key parameter for the runoff modeling) was equal to 84 on average, ranging from 42 to 99. CN map was first derived from the map of the whole of Sardinia Island (made by the regional environmental authority) and then calibrated by comparing runoff predictions and observations. We used the first 65 years (1925–1989) for calibration (Table 5) and the last 33 years for validation. The warm-up period was one year. Yearly runoff predictions were tested successfully (Figure 6 and Table 5; RMSE = 66.01 mm/year, $R^2 = 0.87$, and $p < 0.001$ in calibration, while RMSE = 87.52 mm/year, $R^2 = 0.72$, and $p < 0.001$ in validation. The total predicted runoff of the whole period only had a difference of 10% from that observed). The predicted runoff coefficient was 0.28 on average, ranging from 0.63 in the winter months to 0.20 in dry months, which is close to that observed (RMSE = 0.40, $R^2 = 0.52$, and $p < 0.005$). The model was also validated at a monthly timescale in the Mulargia subbasin for a shorter period due to the availability of the hydrometer data for the 2003–2007 period only, confirming the model's reliability (Figures 6c and 7d; RMSE = 10.42 mm/month, $R^2 = 0.84$, and $p < 0.001$; total predicted runoff of the whole period with a difference of 6.8% from the observed one).

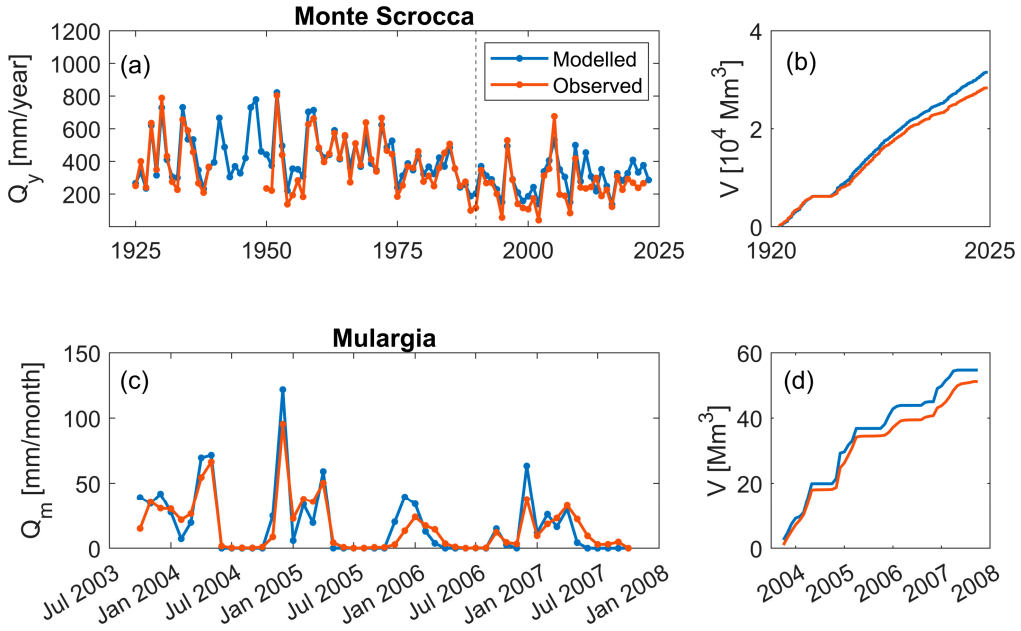

Figure 6. For the historical period, the comparison between observed and modeled runoff of the Flumendosa basin at (**a**) yearly timescale and (**b**) the corresponding cumulative runoff, and of the Mulargia subbasin at (**c**) monthly time scale and (**d**) the corresponding cumulative runoff (values are expressed in millions of cubic meters [mm^3]).

Table 4. Soil-related parameters of the ecohydrological model for the Flumendosa basin.

Parameter	Description	Mean	Range
CN	Curve Number of the Soil Conservation Service method	84	42–99
$\theta_{sat,s}$ [-]	Saturated soil moisture in the surface soil	0.44	0.41–0.46
b_s [-]	Slope of the retention curve in the surface soil	10.28	7.75–11.40
$k_{sat,s}$ [m/s]	Saturated hydraulic conductivity	2.82×10^{-7}	10^{-8}–10^{-6}
d_s [m]	Surface soil depth	0.36	0.20–0.85
$\theta_{sat,r}$ [-]	Saturated moisture in the underlying layer	0.48	0.45–0.50
b_r [-]	Slope of the retention curve in the underlying layer	7	
$k_{sat,r}$ [m/s]	Saturated hydraulic conductivity in the underlying layer	1.41×10^{-7}	5×10^{-9}–5×10^{-7}

Table 5. Runoff prediction evaluation for the calibration and validation periods (RMSE: root mean square error, NSE: Nash–Sutcliffe model efficiency coefficient, ΔV: the variation of the total cumulative runoff volume).

	Monte Scrocca		Mulargia
	Calibration	Validation	Validation
R^2	0.87	0.72	0.84
p	<0.0005	<0.0005	<0.0005
RMSE	66.01 [mm/y]	87.79 [mm/y]	10.42 [mm/m]
NSE	0.84	0.52	0.72
ΔV	11%		6.8%

The model parameters for *ET* predictions were first derived from the literature data and then calibrated for the site. Indeed, we also tested the *ET* predictions with the *ET* observations from the two eddy-covariance stations at Orroli and Nurri, confirming the model's robustness (RMSE = 1.12 mm/d at the Nurri site and RMSE = 0.68 mm/d at the Orroli site; the difference of the total evapotranspiration measured and modeled at a daily timescale is 5.22% at the Orroli site and 4.86% at the Nurri site). The historical trend of predicted basin average ET was not significant (Mann–Kendall $\tau = -0.01$, $p = 0.84$), while

the predicted tree transpiration decreased significantly (Mann–Kendall $\tau = -0.14$, $p < 0.05$). The predicted F_c carbon assimilation decreased significantly (Mann–Kendall $\tau = -0.15$ and $p = 0.01$), and the predicted LAI decreased significantly (Mann–Kendall $\tau = -0.41$ and $p < 0.05$) in the last century.

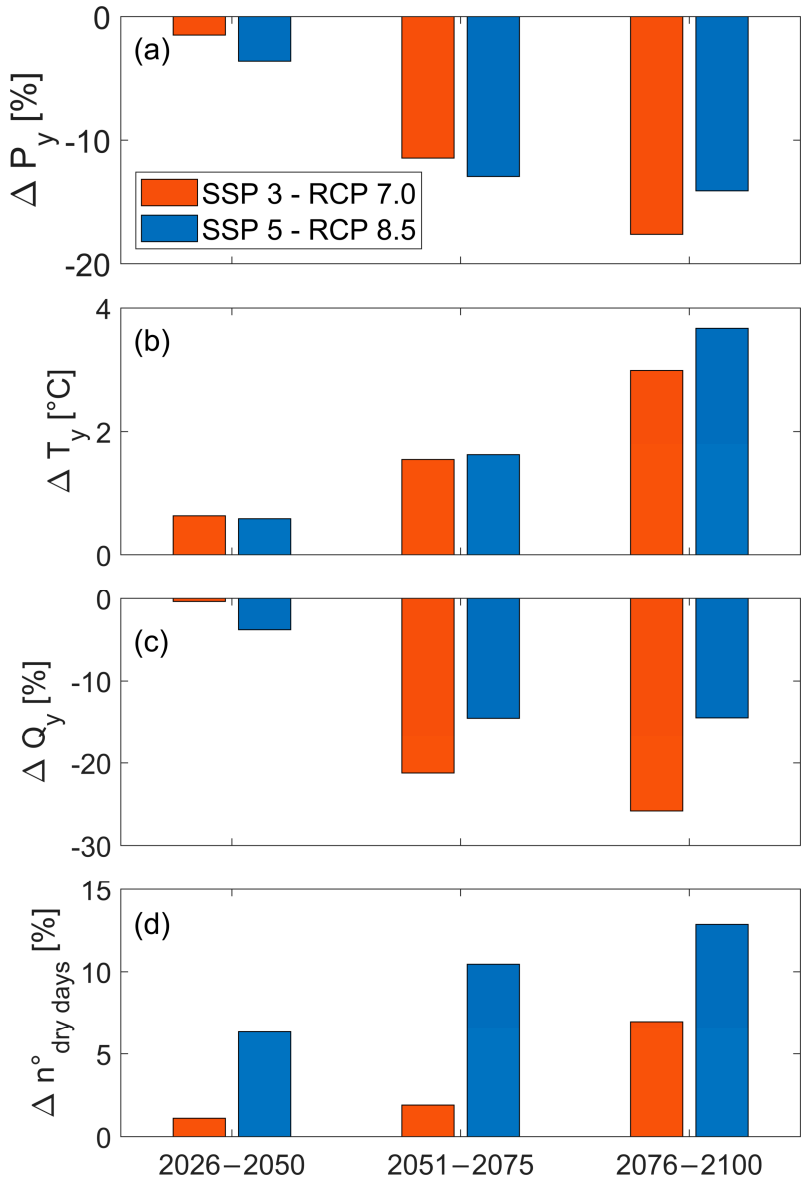

Figure 7. In the Flumendosa basin, mean predicted changes in the future with respect to the historical period of (**a**) annual precipitation (ΔP_y); (**b**) annual air temperature (ΔT_y); (**c**) annual runoff; and (**d**) number of dry days in the year.

We performed a univariate sensitivity analysis of predicted runoff and evapotranspiration to vegetation model parameters for tree and grass ($r_{s,min}$, θ_{lim}, θ_{wp}) and soil model parameter (CN), varying parameter values in a range of ±50% of the calibrated values (which are in Table 1). When we varied the CN parameter, we found the largest effects on predictions of runoff (from −20% to 115% of the runoff). While varying the vegetation parameters, the largest effects were on ET predictions, although lower (from −17% to 15%).

3.3. Future Scenarios of the Water Resources System

Future scenarios of MPI-ESM1-2R-LR predicted a decrease in annual precipitation for the representative concentration pathways SSP3-RCP7.0 and SSP5-RCP8.5, reaching

a decrease of 17.62% for the SSP3-RCP7.0, and 14.10% for the SSP5-RCP8.5 for the period 2076–2100, when compared with the 2001–2025 period (Figure 7a). For future scenarios in the 2076–2100 period, annual air temperature is predicted to increase by ~3 °C for the SSP3-RCP7.0 and ~3.7 °C for the SSP5-RCP8 (Figure 7b). Using the calibrated distributed ecohydrological model, the yearly runoff is predicted to further decrease in most future scenarios, mainly amplifying the rain changes (Figure 7c), reaching the highest decrease of 26% for the SSP3-RCP7.0 configuration in the 2076–2100 period, with a strong decrease in the number of dry days in the year, up to 13% for the SSP5-RCP8.5 and the 2076–2100 period (Figure 7). Combining the effects of the decreasing precipitation and the increasing temperature, the model also predicted a drastic decrease in carbon assimilation: up to −10% for the SSP3-RCP7.0 scenario and −15% for the SSP5-RCP8.5 scenario (for the period 2076–2100). LAI is also predicted to decrease (−10% for the SSP3-RCP7.0 scenario and −15% for the SSP5-RCP8.5 scenario for the period 2076–2100).

Future hydrological predictions have been used to predict the behavior of the water resources management system, considering the civil, industrial, irrigation, and ecological water demands in the WARGI model. Monthly distributions of these water demands have been estimated from historical data and showed an increase in civil demands during the summer months, a strong increase in water demand for irrigation during summer months (up to 22%), an almost constant industrial demand (average 9%), and an increase in ecological water demands in the winter months (Figure S3).

The WARGI model predicted the water volume stored in the reservoir system for the two future climate scenarios and used the three water demand scenarios (Figure 8). With the SSP3-RCP7.0 scenario, the reservoir volume decreased below the reserved volume for civil and industrial demands over several years, which means that irrigation demands could not be satisfied in those months, especially for irrigation scenario C. The number of years of deficit for irrigation increases when the SSP5-RCP8.5 scenario is considered, with extremely low values of stored volume at the end of the twenty-first century, reaching the strategic volume of the dam system for scenario C. This means that, in that dramatic year, domestic water demands will not be satisfied (Figure 8). Figure 9 summarizes the results, distinguishing the number of years of deficit and the mean deficit for each water demand use for the two future scenarios and for water demand scenario C. Irrigation water demands are often not satisfied (up to 74% of years of deficit for the SSP5-RCP8.5 scenario) and the ecological water demands (the minimum water flow) even less so (Figure 9).

We investigated the water resources system for two land cover planning strategies (afforestation/deforestation, see Figure S1) and for the two future emission scenarios under water demand scenario C (Figure 10). The afforestation and deforestation land cover strategies increased and decreased the fraction of tree cover of the basin by 33% and 21%, respectively. We evaluated the variation of the runoff for the three future reference periods (2026–2050, 2051–2075, and 2076–2100) and the two future emission scenarios characterized by a decrease in mean annual wetness conditions, estimating a decrease in runoff with decreasing wetness conditions for the actual cover conditions (Figure 10a). Runoff increased for the future scenarios with basin deforestation, while afforestation activity brought a further decrease in runoff, up to 31% for the SSP5-SSP3-RCP7.0 scenario in the period 2076–2100 (Figure 10a). In contrast, the afforestation will produce a lower decrease in carbon assimilation despite the predicted drier conditions of both future scenarios. During deforestation, the decrease in carbon assimilation will be much higher, up to 40% for the SSP5-RCP8.5 scenario in the period 2076–2100 (Figure 10b). With the deforestation case, WARGI predicted a decrease in the number of deficit years for irrigation, in contrast with the increase in the number of deficit years for irrigation for the afforestation case (Figure 10c).

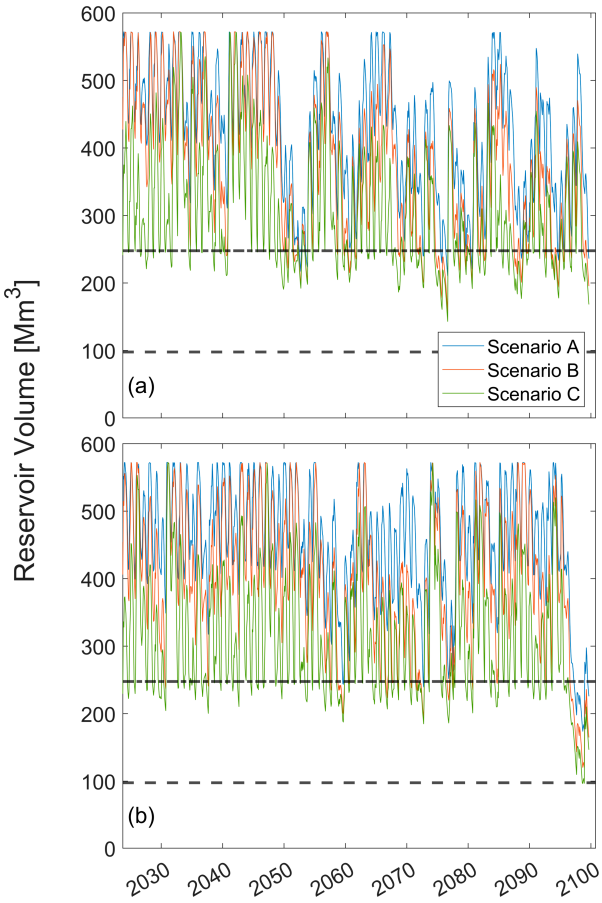

Figure 8. The WARGI model predictions of the water volume stored in the reservoir system using the three water demand scenarios for the (**a**) SSP3-RCP 7.0 future emission scenario and (**b**) SSP5-RCP 8.5 future emission scenario. Dash-dot lines indicate the reserved water volume for civil and industrial water demands, and the dashed lines indicate the strategic water volume that cannot be reached.

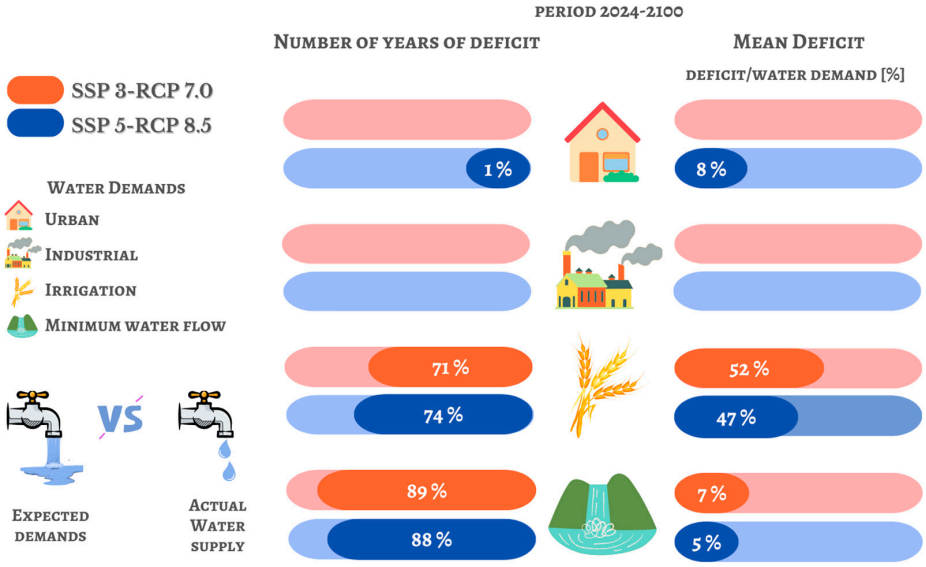

Figure 9. The predicted water deficit for urban, industrial, irrigation, and ecological demands under future emissions scenarios (SSP3-RCP7.0 and SSP5-RCP8.5) and the C demand scenario (Table 3). Note that a year of deficit is when the water demand is not satisfied for more than 15%.

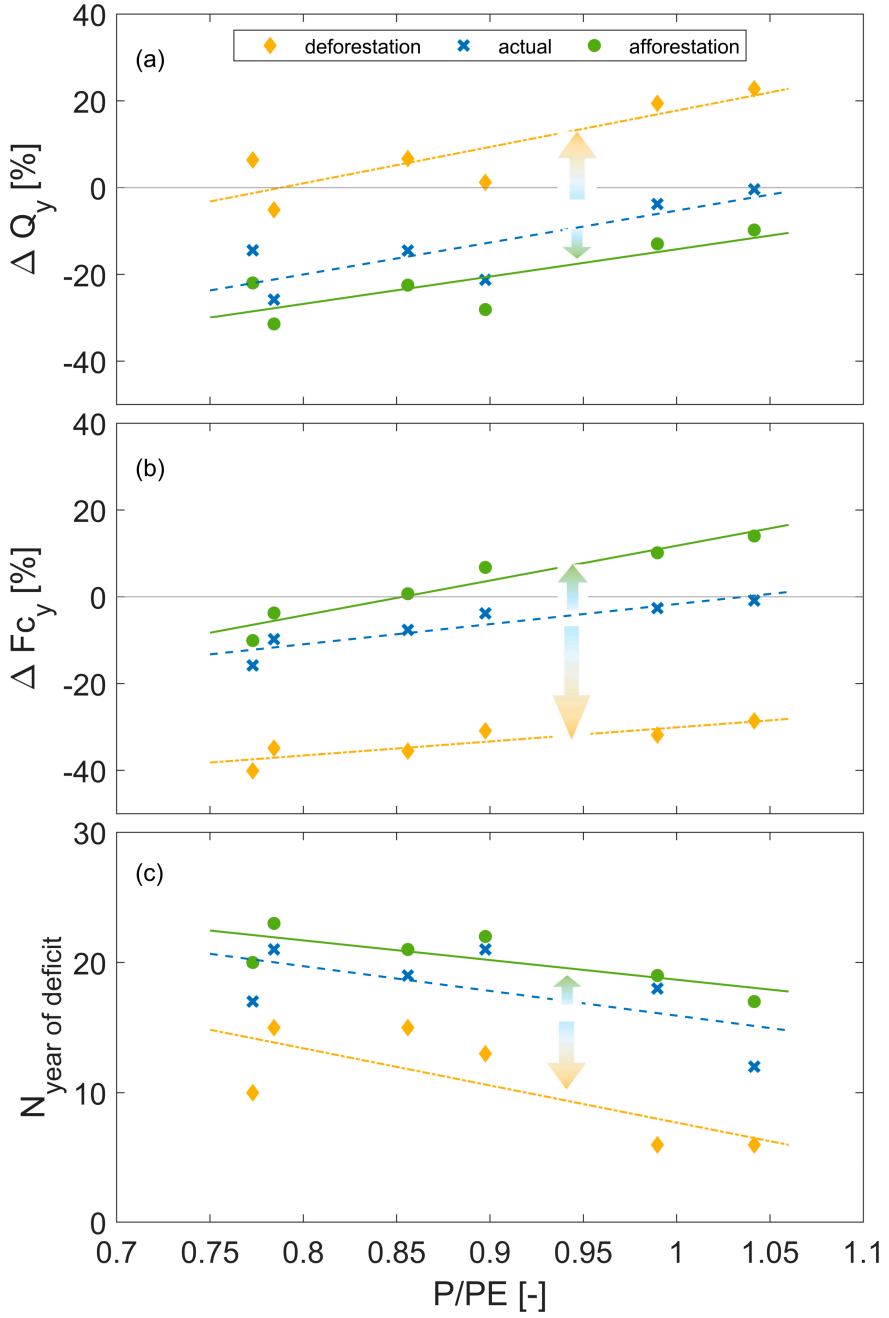

Figure 10. (**a**) The impacts of the land cover change scenarios on runoff (Q_y), (**b**) carbon assimilation (Fc_y), and (**c**) irrigation (number of years of deficit of irrigation) for the different mean annual wetness index (P/PE) of the two future emission scenarios (SSP3-RCP7.0 and SSP5-RCP8.5) and the three future reference periods (2026–2050, 2051–2075, and 2076–2100) under water demand scenario C (Table 3).

Finally, we predicted the number of deficit years for irrigation for three water demand scenarios, one conservative water demand scenario (scenario A), an optimistic water demand scenario (Scenario B), and the C scenario with the highest water demands, considering three land cover planning strategies (afforestation, deforestation, and actual land cover), and under two future emission scenarios (SSP3-RCP7.0 and SSP5-RCP8.5). The full set of strategies under future climate change scenarios provided directions on water demand and land cover planning strategies (Figure 11), with few years of deficit of irrigation (from 4 to 8 years for the actual land cover conditions) for the conservative scenario of

water demand, while with much more years of deficit of irrigation for the B scenario (up to 26 years of deficit of irrigation) and the C scenarios (up to 42 years).

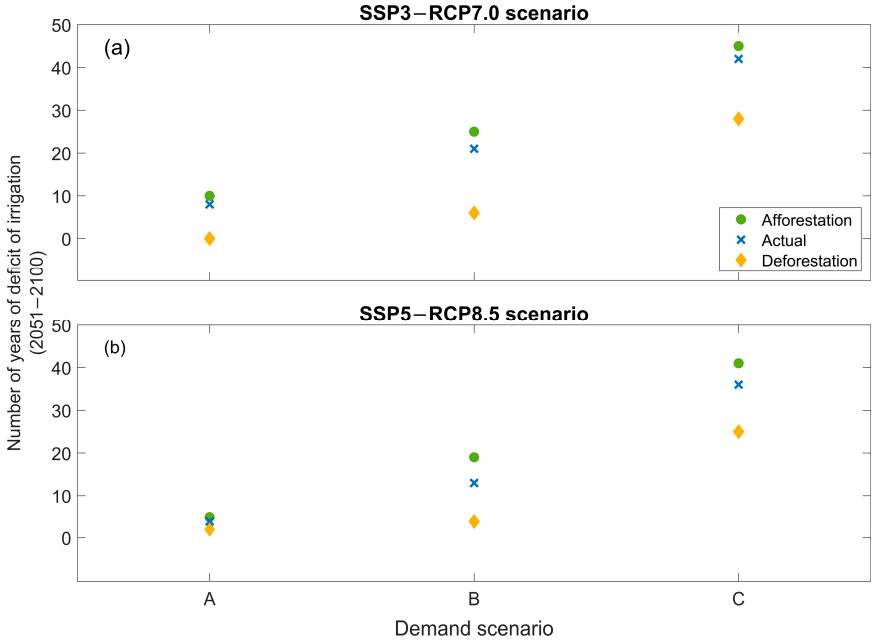

Figure 11. (**a**,**b**) The number of years of deficit of irrigation for the three future water demand scenarios (A, B, and C, details in Table 3), for the future reference period (2051–2100), for three land cover planning strategies (afforestation, actual conditions, and deforestation) under the two future emission scenarios (SSP3-RCP7.0 and SSP5-RCP8.5).

4. Discussion

The Flumendosa basin and its dam system for water resources supply are a key component of the Sardinian water resources system (33% of Sardinia's total reservoir capacity) and is suffering an increase in drought conditions with a historical reduction in winter precipitation (Mann–Kendall $\tau = -0.271$) and an increase in annual air temperature (Mann–Kendall $\tau = +0.373$) since 1923. These results are in agreement with [9], who analyzed all of the Sardinian rainfall data up to 2010, highlighting a large variability of the Mann–Kendall τ for winter precipitation across the island, with an increase in negative Mann–Kendall τ on the west Sardinian coast, where the Flumendosa basin is mainly located, and [24]. Sirigu et al. [24], however, estimated a lower decrease in winter precipitation (Mann–Kendall $\tau = -0.15$) in a smaller basin in the South East of the island. Hurrell et al. [103] demonstrated a clear connection between the persistently positive phase of the North Atlantic Oscillation (NAO) and precipitation reduction in the Mediterranean area. Corona et al. [10] evaluated a strong correlation of the Flumendosa basin winter precipitation with the NAO index (Pearson correlation coefficient of -0.5), highlighting a clear connection between the basin climate and the large-scale NAO dynamics and the representativeness of the basin for the Mediterranean area, with a climate point of view. Sardinia provides an interesting case study of the impacts of climate change because of its position in the center of the Mediterranean Sea, its high sensitivity to climate change [9,11,23,60], its relatively low level of urbanization and human activity (with ~50% of the total area covered by forest [61]), and the lack of relevant land cover changes [24]; the Flumendosa basin is one of the main basins of the Sardinian Island. The strong historical decrease in runoff (Mann–Kendall τ of -0.276) and the simultaneous increase in annual air temperature are testament to the dangerous desertification process in progress in this representative Mediterranean basin, mainly mountainous and historically characterized by a sufficiently high mean annual precipitation (=895 mm). Indeed, one century ago, in the economic development plan of Sardinia, the water resources plan was a key point for the growth of

the island, and the Flumendosa basin was one of the main water resources. A dam system, with a total capacity of 620 × 10^6 m^3, was designed to support the growth of the main city of Sardinia, Cagliari, and the main cultivated area of the island, the Campidano [62,64]. Although the basin did not suffer land cover changes and human impacts in the past, the runoff and, therefore, the recharge of the dam system systematically decreased due to the impact of climate change, causing a rethink of Sardinian water resources planning (last updated in the 1990s [104]). There is a growing need to rethink water resource planning in semi-arid areas with scarce water resources but with favorable conditions for population growth, irrigation, and tourism, such as the countries in the Mediterranean Sea basin, California, and Australia, with a long tradition of adaptation to irregular water resources [42]. Updating water resource planning is even more essential due to the future predictions of the recent IPCC climate scenarios in the Flumendosa basin, which anticipates drier (by an average of 10%, up to 18%) and warmer (by an average of +1.8 °C, up to +3.7 °C) climate conditions (Figure 7), consistent with other findings in the Mediterranean area [15,20]. The use of a distributed ecohydrological model, which simulated almost one hundred years of past data of observed runoff well (Figure 6), allowed us to predict future land surface flux conditions from the IPCC climate scenarios. The downscaling of GCM data at the resolution of 1.25° latitude and 1.87° longitude (~150 km) to the Flumendosa basin scale (~1000 km^2) is subject to uncertainty. However, the use of the multivariate bias correction technique for statistically downscaling GCM future predictions to the basin scale (also at similar spatial scales of the Flumendosa basin) is commonly used for future climate and hydrologic predictions (e.g., [105–107]), and the use of the multivariate bias correction method for the Flumendosa basin was successful, as demonstrated by the high performance of the method when tested with the past data (difference in the mean annual precipitation of 1.95%). Furthermore, the predicted future conditions were similarly observed in other Mediterranean basins ([53], a Turkish basin [48], and Sardinian basins [24,108]. The soil water balance will be modified, with a decrease in infiltration (−8%), soil water content (−4% in the sublayer), and evapotranspiration (−7%). The runoff will further decrease by about 18% (up to 31% for the SSP3-RCP7.0 scenario and the 2076–2100 period) (Figure 10). Water resource planning needs to take these future conditions into account, which highlight a depletion of the basin's water resources that need to match the water demands in the future to maintain sustainability in the system.

Water demands are highly seasonal, and they increase in summer months due to the increase in water usage required for irrigation and civil (including touristic) demands (Figure S3). Hence, the highest water demands coincide with the driest months of the year (Figure 5a), so the collected water in the artificial reservoirs in the wet seasons needs to match the gross summer water use under a multi-year water resource management perspective that needs to prevent possible future repetitive dry years, as included in WARGI [41,86,87]. Irrigation is already the main water demand on the Flumendosa dam system, but we also evaluated the possibility of increasing the irrigation water demands by up to 61% for scenario C. Indeed, while industrial activities are not significantly growing in Sardinia and are not considered a beneficial development choice, the possibility of developing modern agricultural practices is an interesting option for the economic growth of Sardinia, as is typical in Mediterranean growth plans [109,110]. This development strategy needs to be tested in future scenarios in terms of water availability for irrigation.

Due to the WARGI rules of priority for water use in the case of water restrictions, irrigation demands can only be satisfied after civil (first priority) and industrial (second priority) demands, so that, in the future, up to 74% of deficit years are predicted for irrigation, with a mean deficit up to 52% for irrigation scenario C. Hence, in the future, irrigation water demands will not often be satisfied, and irrigation scenario A, which just plans to maintain the actual mean water demands, will be at risk (Figure 8). The only sustainable scenario of water demands for future climate conditions will be a conservative scenario, excluding increases in irrigated areas in southern Sardinia both for the actual conditions of the basin land cover and for the afforestation strategy (Figure 11). The agricultural development for

the growth of the Sardinian economy may be arrested due to the water resources declining, despite the use of optimization criteria for water resources management.

The Flumendosa basin is hydrological sensitive to forest changes ($\Delta Q_y/\Delta f_t$, [59]) with values of 0.4–1.4, which are in agreement with Hou et al. [59] results for water-limited watersheds of small areas. Paradoxically, an extreme land cover change strategy of deforestation could help to increase the availability of water resources in future scenarios (Figure 10) because the decrease of 21% of the forested cover of the basin will lead to an increase in runoff (~7%) and a decrease of 20% of the number of years of irrigation deficit for scenario C. These results agree with several studies [56,111] at a small scale, showing that afforestation reduces runoff. Moreover, deforestation will have a strong impact on the carbon assimilation in the basin, which will decrease by up to 37%; this is definitely not compatible with policies of climate change mitigation and adaptation. Furthermore, in a larger regional and global context, afforestation supplies the atmospheric moisture that becomes precipitation in the hydrologic cycle, increasing water yield. Note that the uncertainty of the future precipitation and temperature data projected by the GCMs have been quantified comparing eleven projections of GCMs (CNRM-CM6-1-ssp-245, CNRM-CM6-1-ssp-585, EC-Earth3-CC-585, EC-Earth-AerChem-370, Hadgem3-ll-126, Hadgem3-ll-245, Hadgem3-ll-585, Hadgem3-mm 585, Mpi-esm1-2lr-sf-126, Mpi-esm1-2r-sf370, Mpi-esm1-2r-sf585) that provided complete datasets for the Sardinian area. The SD for the downscaled average yearly value of precipitation was low (=31.2 mm), and the interquartile range (IQR), which is the difference between 25 and 75 percentiles [112], was also low (=38 mm). Similarly low values of SD and IQR were estimated for the yearly temperature (SD = 1.9 °C, and IQR = 1.7 °C)

The results of the study are limited to a medium-sized Sardinian basin, the Flumendosa basin, which is, however, significant for the Sardinian water resources system. Following the proposed approach, future similar research activities need to be extended to other main Sardinian basins and to other basins along the Mediterranean biome and climate types to identify and compare water resources management and planning strategies for contrasting drier climate conditions in the Mediterranean region. However, these results and the impact of climate change on water resources need to be carefully considered in the Sardinian development plans (and in semi-arid regions in general) because growth policies need to be consistent with mitigating the disastrous effects of human activities on the global climate.

5. Conclusions

The Flumendosa basin case study is characterized by a very attractive long-term (one century) hydrological database, low urbanization, and its key role in the water resources of the Sardinian Island (the Flumendosa reservoir system has a total capacity of about 620×10^6 m^3). It provides an interesting opportunity to analyze the response of water resource systems to historical and future climate change. Historical climate change (1922–2022) is impacting the Flumendosa basin's water resources, with an increase in drought conditions being highlighted by a significant decrease in winter precipitation in the last century (Mann–Kendall $\tau = -0.271$) and an increase in air temperature (Mann–Kendall $\tau = +0.373$). The drier climate conditions of the last 40 years raise questions about the pre-existing regional water resource planning. The proposed distributed ecohydrological model effectively predicted one century of runoff data and became a powerful tool for water resource and environmental planning. We used the spatially distributed ecohydrological model and a water resources management model (WARGI) to define the economic efficiency and the optimal water allocation in the water system configurations throughout the evaluation of multiple planning and management rules for future climate scenarios.

Using the IPCC future climate scenarios (up to the end of the century), the soil is predicted to become drier, with a decrease in infiltration and evapotranspiration (−7%); the runoff will further decrease by about 18%, on average, and up to 31% for 2076–2100 period. In these future hydrological conditions (2024–2100), irrigation demands will not be totally

satisfied, with up to 74% of future years being in deficit for irrigation, with a mean deficit of up to 52% for irrigation scenario C, the scenario with the maximum increase in irrigation in the future. Only a conservative scenario for irrigation, which will exclude the growth of irrigated areas, will be sustainable for the Sardinian water resources system under future climate change scenarios.

We demonstrated that the Flumendosa basin is hydrological sensitive to forest cover changes, as typical of water-limited basins. In this sense, extreme land cover change strategies, such as deforestation, may help to increase water resources in future scenarios but can clearly not be accepted because the deforestation will have a strong impact on the carbon assimilation amount in the basin, which will decrease by up to 37% at the end of the 2076–2100 period, as well as on other environmental factors (e.g., soil erosion control); this is not compatible with policies of climate change mitigation and resilience. Afforestation activities will bring a positive increase in carbon assimilation but a further reduction in runoff, slightly increasing the number of deficit years for irrigation.

These results and the impact of climate change on water resources need to be carefully considered in the Sardinian development plans. Although climate change is caused on a global scale, it impacts water resources and growth at a local scale, with consequences in an island such as Sardinia, which has been a positive example of environmental and natural preservation.

Supplementary Materials: The following supporting information can be downloaded at https://www.mdpi.com/article/10.3390/hydrology11120200/s1, Figure S1: Land cover change scenarios: maps of the fraction of tree vegetation for the: (a) actual basin state; (b) the afforestation scenario; and (c) the deforestation scenario. The fraction of tree cover (ft) is reported for each map; Figure S2: The comparison of 17 Global Climate Models (GCMs) historical predictions with the historical time series of yearly precipitation (Py) and air temperature (Ty). The mean annual variation of the two variables for the period 1983–2014 is compared to the period 1950–1982; Figure S3: Mean monthly water demands in the Flumendosa dam system for civil, industrial, irrigation, and ecological uses; Table S1: Equations of the vegetation dynamic model components. Parameters are defined in the table.

Author Contributions: Conceptualization, N.M.; methodology, N.M.; software, S.S., R.Z. and A.R.; validation, N.M., S.S., R.Z. and A.R; formal analysis, N.M., S.S. and R.C.; investigation, N.M., S.S. and R.C.; resources, N.M.; data curation, S.S. and R.C.; writing—original draft preparation, N.M.; writing—review and editing, N.M.; visualization, S.S.; supervision, N.M.; project administration, N.M.; funding acquisition, N.M. All authors have read and agreed to the published version of the manuscript.

Funding: This work was supported by the Italian Ministry of Education, University and Research (MIUR) through the SWATCH European project of the PRIMA MED program, CUP n. F24D19000010006, the ALTOS project of the PRIMA MED program, CUP n. F24D19000020006, and the FLUXMED project of the WATER JPI program, CUP n. F24D19000030001. We thank the Ente Acque della Sardegna (ENAS) authority for providing data and supporting for the Flumendosa water resources system and ARPAS (the Sardinia regional agency for environmental protection) for providing hydrological data.

Data Availability Statement: The datasets generated during and/or analyzed during the current study are available from the corresponding author upon reasonable request.

Conflicts of Interest: The authors declare no conflicts of interest.

References

1. Brunetti, M.; Maugeri, M.; Nanni, T.; Navarra, A. Droughts and extreme events in regional daily Italian precipitation series. *Int. J. Climatol.* **2002**, *22*, 543–558. [CrossRef]
2. Klein Tank, A.M.G.; Können, G.P. Trends in Indices of Daily Temperature and Precipitation Extremes in Europe, 1946–1999. *J. Clim.* **2003**, *16*, 3665–3680. [CrossRef]
3. Vicente-Serrano, S.M.; Lopez-Moreno, J.I. The influence of atmospheric circulation at different spatial scales on winter drought variability through a semi-arid climatic gradient in Northeast Spain. *Int. J. Climatol.* **2006**, *26*, 1427–1453. [CrossRef]
4. Supari; Tangang, F.; Juneng, L.; Aldrian, E. Observed changes in extreme temperature and precipitation over Indonesia. *Int. J. Climatol.* **2017**, *37*, 1979–1997. [CrossRef]

5. Sharma, A.; Goyal, M. Assessment of the changes in precipitation and temperature in Teesta River basin in Indian Himalayan Region under climate change. *Atmos. Res.* **2020**, *231*, 104670. [CrossRef]
6. Giorgi, F. Climate change hot-spots. *Geophys. Res. Lett.* **2006**, *33*, 101029. [CrossRef]
7. Cudennec, C.; Leduc, C.; Koutsoyiannis, D. Dryland hydrology in Mediterranean regions—A review. *Hydrol. Sci. J.* **2007**, *52*, 1077–1087. [CrossRef]
8. Martinez-Fernandez, J.; Sanchez, N.; Herrero-Jimenez, C.M. Recent trends in rivers with near-natural flow regime: The case of the river headwaters in Spain. *Prog. Phys. Geogr.* **2013**, *37*, 685–700. [CrossRef]
9. Montaldo, N.; Sarigu, A. Potential links between the North Atlantic Oscillation and decreasing precipitation and runoff on a Mediterranean area. *J. Hydrol.* **2017**, *553*, 419–437. [CrossRef]
10. Corona, R.; Montaldo, N.; Albertson, J.D. On the Role of NAO-Driven Interannual Variability in Rainfall Seasonality on Water Resources and Hydrologic Design in a Typical Mediterranean Basin. *J. Hydrometeorol.* **2018**, *19*, 485–498. [CrossRef]
11. Montaldo, N.; Oren, R. Changing Seasonal Rainfall Distribution With Climate Directs Contrasting Impacts at Evapotranspiration and Water Yield in the Western Mediterranean Region. *Earth Future* **2018**, *6*, 841–856. [CrossRef]
12. Savenije, H. The runoff coefficient as the key to moisture recycling. *J. Hydrol.* **1996**, *176*, 219–225. [CrossRef]
13. Oki, T.; Agata, Y.; Kanae, S.; Saruhashi, T.; Yang, D.; Musiake, K. Global assessment of current water resources using total runoff integrating pathways. *Hydrol. Sci. J.* **2001**, *46*, 983–995. [CrossRef]
14. Statzu, V.; Strazzera, E. *Water Demand for Residential Uses in a Mediterranean Region: Econometric Analysis and Policy Implications*; University of Cagliari: Cagliari, Italy, 2009.
15. Ozturk, T.; Ceber, Z.P.; Turkes, M.; Kurnaz, M.L. Projections of climate change in the Mediterranean Basin by using downscaled global climate model outputs. *Int. J. Climatol.* **2015**, *35*, 4276–4292. [CrossRef]
16. Lionello, P.; Scarascia, L. The relation between climate change in the Mediterranean region and global warming. *Reg. Envir. Chang.* **2018**, *18*, 1481–1493. [CrossRef]
17. Carvalho, D.; Pereira, S.; Silva, R.; Rocha, A. Aridity and desertification in the Mediterranean under EURO-CORDEX future climate change scenarios. *Clim. Chang.* **2022**, *174*, 28. [CrossRef]
18. Cos, J.; Doblas-Reyes, F.; Jury, M.; Marcos, R.; Bretonnière, P.; Samsó, M. The Mediterranean climate change hotspot in the CMIP5 and CMIP6 projections. *Earth Syst. Dynam.* **2022**, *13*, 321–340. [CrossRef]
19. Mariotti, A.; Zeng, N.; Yoon, J.-H.; Artale, V.; Navarra, A.; Alpert, P.; Li, L.Z. Mediterranean water cycle changes: Transition to drier 21st century conditions in observations and CMIP3 simulations. *Environ. Res. Lett.* **2008**, *3*, 044001. [CrossRef]
20. May, W. Potential future changes in the characteristics of daily precipitation in Europe simulated by the HIRHAM regional climate model. *Clim. Dyn.* **2008**, *30*, 581–603. [CrossRef]
21. Mastrandrea, M.D.; Luers, A.L. Climate change in California: Scenarios and approaches for adaptation. *Clim. Chang.* **2012**, *111*, 5–16. [CrossRef]
22. Masseroni, D.; Camici, S.; Cislaghi, A.; Vacchiano, G.; Massari, C.; Brocca, L. The 63-year changes in annual streamflow volumes across Europe with a focus on the Mediterranean basin. *Hydrol. Earth Syst. Sci.* **2021**, *25*, 5589–5601. [CrossRef]
23. Marras, P.A.; Lima, D.C.A.; Soares, P.M.M.; Cardoso, R.M.; Medas, D.; Dore, E.; De Giudici, G. Future precipitation in a Mediterranean island and streamflow changes for a small basin using EURO-CORDEX regional climate simulations and the SWAT model. *J. Hydrol.* **2021**, *603*, 127025. [CrossRef]
24. Sirigu, S.; Montaldo, N. Climate Change Impacts on the Water Resources and Vegetation Dynamics of a Forested Sardinian Basin through a Distributed Ecohydrological Model. *Water* **2022**, *14*, 3078. [CrossRef]
25. Hawtree, D.; Nunes, J.; Keizer, J.; Jacinto, R.; Santos, J.; Rial-Rivas, M.; Boulet, A.; Tavares-Wahren, F.; Feger, K. Time series analysis of the long-term hydrologic impacts of afforestation in the Agueda watershed of north-central Portugal. *Hydrol. Earth Syst. Sci.* **2015**, *19*, 3033–3045. [CrossRef]
26. Guyennon, N.; Salerno, F.; Rossi, D.; Rainaldi, M.; Calizza, E.; Romano, E. Climate change and water abstraction impacts on the long-term variability of water levels in Lake Bracciano (Central Italy): A Random Forest approach. *J. Hydrol.-Reg. Stud.* **2021**, *37*, 100880. [CrossRef]
27. Zanoni, M.; Stella, E.; Bellin, A. Long-term hydrological behavior of an Alpine glacier. *J. Hydrol.* **2023**, *626*, 130316. [CrossRef]
28. Barbeta, A.; Mejia-Chang, M.; Ogaya, R.; Voltas, J.; Dawson, T.E.; Penuelas, J. The combined effects of a long-term experimental drought and an extreme drought on the use of plant-water sources in a Mediterranean forest. *Glob. Chang. Biol.* **2015**, *21*, 1213–1225. [CrossRef]
29. Clark, P.U.; Shakun, J.D.; Marcott, S.A.; Mix, A.C.; Eby, M.; Kulp, S.; Levermann, A.; Milne, G.A.; Pfister, P.L.; Santer, B.D.; et al. Consequences of twenty-first-century policy for multi-millennial climate and sea-level change. *Nat. Clim. Chang.* **2016**, *6*, 360–369. [CrossRef]
30. Arora, V.K. Simulating energy and carbon fluxes over winter wheat using coupled land surface and terrestrial ecosystem models. *Agric. For. Meteorol.* **2003**, *118*, 21–47. [CrossRef]
31. Montaldo, N.; Rondena, R.; Albertson, J.D.; Mancini, M. Parsimonious modeling of vegetation dynamics for ecohydrologic studies of water-limited ecosystems. *Water Resour. Res.* **2005**, *41*, W10416. [CrossRef]
32. Ivanov, V.Y.; Bras, R.L.; Vivoni, E.R. Vegetation-hydrology dynamics in complex terrain of semiarid areas: 2. Energy-water controls of vegetation spatiotemporal dynamics and topographic niches of favorability. *Water Resour. Res.* **2008**, *44*, W03430. [CrossRef]

33. Montaldo, N.; Albertson, J.D.; Mancini, M. Vegetation dynamics and soil water balance in a water-limited Mediterranean ecosystem on Sardinia, Italy. *Hydrol. Earth Syst. Sci.* **2008**, *12*, 1257–1271. [CrossRef]
34. Schilling, K.E.; Jha, M.K.; Zhang, Y.-K.; Gassman, P.W.; Wolter, C.F. Impact of land use and land cover change on the water balance of a large agricultural watershed: Historical effects and future directions. *Water Resour. Res.* **2008**, *44*, W00A09. [CrossRef]
35. Touhami, I.; Chirino, E.; Andreu, J.; Sánchez, J.; Moutahir, H.; Bellot, J. Assessment of climate change impacts on soil water balance and aquifer recharge in a semiarid region in south east Spain. *J. Hydrol.* **2015**, *527*, 619–629. [CrossRef]
36. Yin, Z.; Feng, Q.; Zou, S.; Yang, L. Assessing variation in water balance components in mountainous inland river basin experiencing climate change. *Water* **2016**, *8*, 472. [CrossRef]
37. Swart, N.; Cole, J.; Kharin, V.; Lazare, M.; Scinocca, J.; Gillett, N.; Anstey, J.; Arora, V.; Christian, J.; Hanna, S.; et al. *CCCma CanESM5 Model Output Prepared for CMIP6 C4MIP*; World Data Center for Climate (WDCC) at DKRZ: Hamburg, Germany, 2019; Volume 12, pp. 4823–4873. [CrossRef]
38. Gustafson, E.J.; De Bruijn, A.M.; Pangle, R.E.; Limousin, J.M.; McDowell, N.G.; Pockman, W.T.; Sturtevant, B.R.; Muss, J.D.; Kubiske, M.E. Integrating ecophysiology and forest landscape models to improve projections of drought effects under climate change. *Glob. Chang. Biol.* **2015**, *21*, 843–856. [CrossRef]
39. Noce, S.; Collalti, A.; Santini, M. Likelihood of changes in forest species suitability, distribution, and diversity under future climate: The case of Southern Europe. *Ecol. Evol.* **2017**, *7*, 9358–9375. [CrossRef]
40. Pinheiro, E.A.R.; Van Lier, Q.D.J.; Bezerra, A.H.F. Hydrology of a Water-Limited Forest under Climate Change Scenarios: The Case of the Caatinga Biome, Brazil. *Forests* **2017**, *8*, 62. [CrossRef]
41. Sulis, A.; Sechi, G. Comparison of generic simulation models for water resource systems. *Environ. Modell. Softw.* **2013**, *40*, 214–225. [CrossRef]
42. Garrote, L. Managing Water Resources to Adapt to Climate Change: Facing Uncertainty and Scarcity in a Changing Context. *Water Resour. Manag.* **2017**, *31*, 2951–2963. [CrossRef]
43. Han, X.; Boota, M.; Soomro, S.; Ali, S.; Soomro, S.; Soomro, N.; Soomro, M.; Soomro, A.; Batool, S.; Bai, Y.; et al. Water strategies and management: Current paths to sustainable water use. *Appl. Water Sci.* **2024**, *14*, 154. [CrossRef]
44. Qin, Y.; Wang, C.; Zhao, Z.; Pan, X.; Li, Z. Climate change impacts on the global potential geographical distribution of the agricultural invasive pest, *Bactrocera dorsalis* (Hendel) (Diptera: Tephritidae). *Clim. Chang.* **2019**, *155*, 145–156. [CrossRef]
45. Eekhout, J.; Delsman, I.; Baartman, J.; van Eupen, M.; van Haren, C.; Contreras, S.; Martínez-López, J.; de Vente, J. How future changes in irrigation water supply and demand affect water security in a Mediterranean catchment. *Agric. Water Manag.* **2024**, *297*, 108818. [CrossRef]
46. Lyra, A.; Loukas, A. Simulation and Evaluation of Water Resources Management Scenarios Under Climate Change for Adaptive Management of Coastal Agricultural Watersheds. *Water Resour. Manag.* **2023**, *37*, 2625–2642. [CrossRef]
47. Koch, H.; Silva, A.; Liersch, S.; de Azevedo, J.; Hattermann, F. Effects of model calibration on hydrological and water resources management simulations under climate change in a semi-arid watershed. *Clim. Chang.* **2020**, *163*, 1247–1266. [CrossRef]
48. Gorguner, M.; Kavvas, M.L. Modeling impacts of future climate change on reservoir storages and irrigation water demands in a Mediterranean basin. *Sci. Total Environ.* **2020**, *748*, 141246. [CrossRef]
49. Beça, P.; Rodrigues, A.; Nunes, J.; Diogo, P.; Mujtaba, B. Optimizing Reservoir Water Management in a Changing Climate. *Water Resour. Manag.* **2023**, *37*, 3423–3437. [CrossRef]
50. Garrote, L.; Granados, A.; Spiliotis, M.; Martin-Carrasco, F. Effectiveness of Adaptive Operating Rules for Reservoirs. *Water Resour. Manag.* **2023**, *37*, 2527–2542. [CrossRef]
51. Latron, J.; Gallart, F. Seasonal dynamics of runoff-contributing areas in a small Mediterranean research catchment (Vallcebre, Eastern Pyrenees). *J. Hydrol.* **2007**, *335*, 194–206. [CrossRef]
52. Fortesa, J.; Latron, J.; Garcia-Comendador, J.; Tomas-Burguera, M.; Company, J.; Calsamiglia, A.; Estrany, J. Multiple Temporal Scales Assessment in the Hydrological Response of Small Mediterranean-Climate Catchments. *Water* **2020**, *12*, 299. [CrossRef]
53. Garcia-Ruiz, J.M.; Lopez-Moreno, J.I.; Vicente-Serrano, S.M.; Lasanta-Martinez, T.; Begueria, S. Mediterranean water resources in a global change scenario. *Earth-Sci. Rev.* **2011**, *105*, 121–139. [CrossRef]
54. Guerra, C.A.; Maes, J.; Geijzendorffer, I.; Metzger, M.J. An assessment of soil erosion prevention by vegetation in Mediterranean Europe: Current trends of ecosystem service provision. *Ecol. Indic.* **2016**, *60*, 213–222. [CrossRef]
55. Zhang, L.; Dawes, W.R.; Walker, G.R. Response of mean annual evapotranspiration to vegetation changes at catchment scale. *Water Resour. Res.* **2001**, *37*, 701–708. [CrossRef]
56. Ellison, D.; Futter, M.N.; Bishop, K. On the forest cover–water yield debate: From demand-to supply-side thinking. *Glob. Chang. Biol.* **2012**, *18*, 806–820. [CrossRef]
57. Filoso, S.; Bezerra, M.; Weiss, K.; Palmer, M. Impacts of forest restoration on water yield: A systematic review. *PLoS ONE* **2017**, *12*, e0183210. [CrossRef]
58. Ovando, P.; Beguería, S.; Campos, P. Carbon sequestration or water yield? The effect of payments for ecosystem services on forest management decisions in Mediterranean forests. *Water Resour. Econ.* **2019**, *28*, 100119. [CrossRef]
59. Hou, Y.; Wei, X.; Zhang, M.; Creed, I.; McNulty, S.; Ferraz, S. A global synthesis of hydrological sensitivities to deforestation and forestation. *For. Ecol. Manag.* **2023**, *529*, 120718. [CrossRef]
60. Piras, M.; Mascaro, G.; Deidda, R.; Vivoni, E.R. Quantification of hydrologic impacts of climate change in a Mediterranean basin in Sardinia, Italy, through high-resolution simulations. *Hydrol. Earth Syst. Sci.* **2014**, *18*, 5201–5217. [CrossRef]

61. Salis, M.; Ager, A.A.; Alcasena, F.J.; Arca, B.; Finney, M.A.; Pellizzaro, G.; Spano, D. Analyzing seasonal patterns of wildfire exposure factors in Sardinia, Italy. *Environ. Monit. Assess.* **2015**, *187*, 4175. [CrossRef]
62. Vinelli, M. Water conservation in Sardinia. *Geogr. Rev.* **1926**, *16*, 395–402. [CrossRef]
63. Sechi, G.; Zucca, R.; Zuddas, P. Water Costs Allocation in Complex Systems Using a Cooperative Game Theory Approach. *Water Resour. Manag.* **2013**, *27*, 1781–1796. [CrossRef]
64. Dozier, C.L. Establishing a Framework for Development in Sardinia: The Campidano. *Geogr. Rev.* **1957**, *47*, 490–506. [CrossRef]
65. Corsale, A.; Iorio, M. Recent trends in water policy in Sardinia. Filling the gap between increased demand and decreasing availability. In *Global Changes: Vulnerability, Mitigation and Adataption*; Sofia University Press-Za Bukvite: Tokyo, Japan, 2009; pp. 435–440.
66. Montaldo, N.; Corona, R.; Albertson, J.D. On the separate effects of soil and land cover on Mediterranean ecohydrology: Two contrasting case studies in Sardinia, Italy. *Water Resour. Res.* **2013**, *49*, 1123–1136. [CrossRef]
67. Montaldo, N.; Corona, R.; Curreli, M.; Sirigu, S.; Piroddi, L.; Oren, R. Rock water as a key resource for patchy ecosystems on shallow soils: Digging deep tree clumps subsidize surrounding surficial grass. *Earth's Future* **2021**, *9*, e2020EF001870. [CrossRef]
68. Yu, K.L.; D'Odorico, P. Climate, vegetation, and soil controls on hydraulic redistribution in shallow tree roots. *Adv. Water Resour.* **2014**, *66*, 70–80. [CrossRef]
69. Noilhan, J.; Planton, S. A Simple Parameterization of Land Surface Processes for Meteorological Models. *Mon. Weather Rev.* **1989**, *117*, 536–549. [CrossRef]
70. Service, S.C. *National Engineering Handbook, Section 4: Hydrology*; Department of Agriculture: Washington, DC, USA, 1986.
71. Service, S.C. *National Engineering Handbook, Section 4: Hydrology*; Department of Agriculture: Washington, DC, USA, 1972.
72. Chow, V.; Maidment, D.; Mays, L. *Applied Hydrology*; McGraw-Hill Book Company: New York, NY, USA, 1988.
73. Ponce, V.M. *Engineering Hydrology: Principles and Practices*; Prentice Hall: Hoboken, NJ, USA, 1989.
74. Albertson, J.D.; Kiely, G. On the structure of soil moisture time series in the context of land surface models. *J. Hydrol.* **2001**, *243*, 101–119. [CrossRef]
75. Clapp, R.B.; Hornberger, G.M. Empirical equations for some soil hydraulic properties. *Water Resour. Res.* **1978**, *14*, 601–604. [CrossRef]
76. Ryel, R.; Caldwell, M.; Yoder, C.; Or, D.; Leffler, A. Hydraulic redistribution in a stand of Artemisia tridentata: Evaluation of benefits to transpiration assessed with a simulation model. *Oecologia* **2002**, *130*, 173–184. [CrossRef]
77. Brutsaert, W. *Evaporation into the Atmosphere: Theory, History, and Applications*; Kluwer Academic Publishers: Dordrecht, The Netherlands, 1982.
78. Jarvis, P.G.; Monteith, J.L.; Weatherley, P.E. The interpretation of the variations in leaf water potential and stomatal conductance found in canopies in the field. *Philos. Trans. R. Soc. Lond. B Biol. Sci.* **1976**, *273*, 593–610. [CrossRef]
79. Parlange, M.B.; Hopmans, J.W. *Evaporation. Use of Fast-Response Turbulence Sensors, Raman Lidar, and Passive Microwave Remote Sensing*; Oxford Academic: Oxford, UK, 1999; pp. 260–278. [CrossRef]
80. Brutsaert, W. *Evaporation into the Atmosphere: Theory, History and Applications*; Springer Science & Business Media: Berlin/Heidelberg, Germany, 2013; Volume 1.
81. Larcher, W. *Physiological Plant Ecology*, 3rd ed.; Springer: Berlin/Heidelberg, Germany, 1995.
82. Cayrol, P.; Chehbouni, A.; Kergoat, L.; Dedieu, G.; Mordelet, P.; Nouvellon, Y. Grassland modeling and monitoring with SPOT-4 VEGETATION instrument during the 1997-1999 SALSA experiment. *Agric. For. Meteorol.* **2000**, *105*, 91–115. [CrossRef]
83. Nouvellon, Y.; Rambal, S.; Lo Seen, D.; Moran, M.S.; Lhomme, J.P.; Begue, A.; Chehbouni, A.G.; Kerr, Y. Modelling of daily fluxes of water and carbon from shortgrass steppes. *Agric. For. Meteorol.* **2000**, *100*, 137–153. [CrossRef]
84. Montaldo, N.; Ravazzani, G.; Mancini, M. On the prediction of the Toce alpine basin floods with distributed hydrologic models. *Hydrol. Process.* **2007**, *21*, 608–621. [CrossRef]
85. Sorooshian, S. Surface water hydrology: On-line estimation. *Rev. Geophys.* **1983**, *21*, 706–721. [CrossRef]
86. Sechi, G.; Zuddas, P. WARGI: Water resources system optimisation aided by graphical interface. In Proceedings of the Hydraulic Engeneering Software VIII, Ashrust, UK, 1 January 2000; pp. 109–120.
87. Sechi, G.; Sulis, A. Water System Management through a Mixed Optimization-Simulation Approach. *J. Water Resour. Plan. Manag.-ASCE* **2009**, *135*, 160–170. [CrossRef]
88. Detto, M.; Montaldo, N.; Albertson, J.D.; Mancini, M.; Katul, G. Soil moisture and vegetation controls on evapotranspiration in a heterogeneous Mediterranean ecosystem on Sardinia, Italy. *Water Resour. Res.* **2006**, *42*, 16. [CrossRef]
89. Montaldo, N.; Curreli, M.; Corona, R.; Oren, R. Fixed and variable components of evapotranspiration in a Mediterranean wild-olive—Grass landscape mosaic. *Agric. For. Meteorol.* **2020**, *280*, 107769. [CrossRef]
90. Hersbach, H.; Bell, B.; Berrisford, P.; Hirahara, S.; Horányi, A.; Muñoz-Sabater, J.; Nicolas, J.; Peubey, C.; Radu, R.; Schepers, D.; et al. The ERA5 global reanalysis. *Q. J. R. Meteorol. Soc.* **2020**, *146*, 1999–2049. [CrossRef]
91. Hersbach, H.; Bell, B.; Berrisford, P.; Biavati, G.; Horányi, A.; Muñoz Sabater, J.; Nicolas, J.; Peubey, C.; Radu, R.; Rozum, I.; et al. ERA5 hourly data on single levels from 1940 to present. *Copernicus Climate Change Service (C3S) Climate Data Store (CDS)*. [CrossRef]
92. Eyring, V.; Bony, S.; Meehl, G.; Senior, C.; Stevens, B.; Stouffer, R.; Taylor, K. Overview of the Coupled Model Intercomparison Project Phase 6 (CMIP6) experimental design and organization. *Geosci. Model Dev.* **2016**, *9*, 1937–1958. [CrossRef]

93. Cannon, A.J. Multivariate quantile mapping bias correction: An *N*-dimensional probability density function transform for climate model simulations of multiple variables. *Clim. Dyn.* **2018**, *50*, 31–49. [CrossRef]
94. Kendall, M.G. A new measure of rank correlation. *Biometrika* **1938**, *30*, 81–93. [CrossRef]
95. Sneyers, R. *On the Statistical Analysis of Series of Observations*; CABI: São Paulo, Brazil, 1991.
96. Hensel, D.; Hirsch, R. *Statistical Method in Water Resources*; USGS Science for a Changing World: Reston, VA, USA, 2002; Chapter A3.
97. Theil, H. A rank-invariant method of linear and polynomial regression analysis. *Indag. Math.* **1950**, *1*, 173.
98. Sen, P.K. Estimates of the Regression Coefficient Based on Kendall's Tau. *J. Am. Stat. Assoc.* **1968**, *63*, 1379–1389. [CrossRef]
99. Hirsch, R.M.; Slack, J.R.; Smith, R.A. Techniques of trend analysis for monthly water quality data. *Water Resour. Res.* **1982**, *18*, 107–121. [CrossRef]
100. Mohsin, T.; Gough, W.A. Trend analysis of long-term temperature time series in the Greater Toronto Area (GTA). *Theor. Appl. Climatol.* **2010**, *101*, 311–327. [CrossRef]
101. Hu, Y.; Maskey, S.; Uhlenbrook, S. Trends in temperature and rainfall extremes in the Yellow River source region, China. *Clim. Chang.* **2012**, *110*, 403–429. [CrossRef]
102. Amirabadizadeh, M.; Huang, Y.F.; Lee, T.S. Recent trends in temperature and precipitation in the Langat River Basin, Malaysia. *Adv. Meteorol.* **2015**, *2015*, 579437. [CrossRef]
103. Hurrell, J.W. Decadal Trends in the North Atlantic Oscillation: Regional Temperatures and Precipitation. *Science* **1995**, *269*, 676–679. [CrossRef]
104. Pinna, C.C.; Silvano, R.; Fadda, A. *Nuovo Studio Dell'idrologia Superficiale della Sardegna*; Ente Autonomo del Flumendosa: Cagliari, Italy, 1998.
105. Adeyeri, O.; Laux, P.; Lawin, A.; Oyekan, K. Multiple bias-correction of dynamically downscaled CMIP5 climate models temperature projection: A case study of the transboundary Komadugu-Yobe river basin, Lake Chad region, West Africa. *SN Appl. Sci.* **2020**, *2*, 1221. [CrossRef]
106. Miralha, L.; Muenich, R.; Scavia, D.; Wells, K.; Steiner, A.; Kalcic, M.; Apostel, A.; Basile, S.; Kirchhoff, C. Bias correction of climate model outputs influences watershed model nutrient load predictions. *Sci. Total Environ.* **2021**, *759*, 143039. [CrossRef]
107. El-Samra, R.; Haddad, A.; Alameddine, I.; Bou-Zeid, E.; El-Fadel, M. Downscaling Climatic Variables at a River Basin Scale: Statistical Validation and Ensemble Projection under Climate Change Scenarios. *Climate* **2024**, *12*, 27. [CrossRef]
108. Pulighe, G.; Lupia, F.; Chen, H.; Yin, H. Modeling Climate Change Impacts on Water Balance of a Mediterranean Watershed Using SWAT+. *Hydrology* **2021**, *8*, 157. [CrossRef]
109. Llop, M.; Ponce-Alifonso, X. Water and Agriculture in a Mediterranean Region: The Search for a Sustainable Water Policy Strategy. *Water* **2016**, *8*, 66. [CrossRef]
110. Zdruli, P. Land Resources of the Mediterranean: Status, pressure, trends and impacts on future regional developement. *Land Degrad. Dev.* **2014**, *25*, 373–384. [CrossRef]
111. Andréassian, V. Waters and forests:: From historical controversy to scientific debate. *J. Hydrol.* **2004**, *291*, 1–27. [CrossRef]
112. Song, Y.; Chung, E.; Shiru, M. Uncertainty Analysis of Monthly Precipitation in GCMs Using Multiple Bias Correction Methods under Different RCPs. *Sustainability* **2020**, *12*, 7508. [CrossRef]